REVIEW

Thermal Analysis and Thermal Reactions of Smectites: a Review of Methodology, Mechanisms, and Kinetics

Arkadiusz Derkowski · Artur Kuligiewicz

© The Author(s) 2023

Abstract Smectites are a group of minerals traditionally analyzed by thermal methods due to their exceptionally large adsorbed-water contents and the presence of OH groups, which makes them unique among all common soil- and rock-forming minerals. The dehydration reaction of smectite is a low-temperature endothermic effect that ends typically below 200°C. Although the removal of bulk interlayer water requires activation energy (E_a) of just above 30 kJ/mol, the removal of the last few H_2O molecules attached strongly to interlayer cations requires $E_a > 100$ kJ/mol. Dehydroxylation is the loss of structural OH groups that proceeds as evolution of H_2O molecules out of the smectite structure and occurs in the 300–900°C range. In trioctahedral species, dehydroxylation is combined with recrystallization and proceeds usually at > 700°C. In dioctahedral species, the temperature of dehydroxylation is controlled by the type of octahedral vacancy, having *trans-vacant* and *cis-vacant* distinguished by the boundary at ~600°C, and by the octahedral cation–OH bond strength, following the order Mg > Al > Fe. The E_a of dehydroxylation correlates linearly with the temperature of maximum dehydroxylation; from > 170 kJ/mol for Cs$^+$-exchanged beidellite and nontronite, through ~300 kJ/mol in Mg-rich montmorillonite, to > 500 kJ/mol in trioctahedral saponite. Dehydration and dehydroxylation of smectites can be accompanied by a number of other phenomena, such as dehydrogenation or defluorination. At high temperatures, smectite amorphization and recrystallization occurs. Unless amorphized and/or recrystallized, smectites can undergo rehydration and rehydroxylation, which are opposite reactions to dehydration and dehydroxylation, respectively. This review discusses the details of the above-mentioned thermal reactions of smectites, focusing on thermogravimetric methods, evolved gas analysis, and structural alterations. Factors affecting the accuracy and precision of thermal analysis of smectite are discussed along with examples of best laboratory practices. The paper also provides the most recent description and critical evaluation of smectite reaction kinetics.

Keywords Activation energy · Dehydration · Dehydroxylation · Reaction kinetics · Smectite · Thermal analysis

A. Derkowski (✉) · A. Kuligiewicz
Institute of Geological Sciences, Polish Academy of Sciences, Senacka 1, 31-002 Krakow, Poland
e-mail: ndderkow@cyf-kr.edu.pl

Introduction

Thermal analysis is the oldest instrumental method applied to clays and clay minerals. The first application of thermal analysis to classify and identify smectitic species (Le Chatelier, 1887) happened long before the discovery of

X-ray radiation and the identification of the actual smectite structure using X-ray diffractometry (XRD). Right after the description of the smectite structure by Hofman et al. (1933), the already-developed differential thermal analysis (DTA) methodology quickly become a major tool in studying smectites, along with their classification and transformations (Grim & Bradley, 1940; Grim & Rowland, 1942a, b). Already in the early years of investigation, the nature of the main DTA peaks in a smectite heating curve had been identified correctly: the low-temperature endothermic DTA peak is caused by dehydration and the high-temperature endothermic DTA peak is caused by dehydroxylation (Fig. 1). These two reactions are followed by structure decomposition and recrystallization.

Thermal Analysis Methodology

Thermal analysis is a ubiquitous and widely used general term that refers to a number of analytical methods monitoring the change in a material's property with temperature, usually measured over small intervals of time or temperature change. The principles and various methods have been described in numerous reviews and books (Byrn et al., 2017; Gabbott, 2008; Plante et al., 2009), including excellent, in-depth reviews devoted specifically to clay minerals (Emmerich, 2010; Stucki et al., 1990). Therefore, the present paper focuses only on the application of thermal analysis to smectites (also applicable to vermiculites and smectite-interstratified phases) and only to smectites in a form corresponding to their most common natural occurrence in rocks and sediments, i.e. having inorganic interlayer cations. Thermal analysis
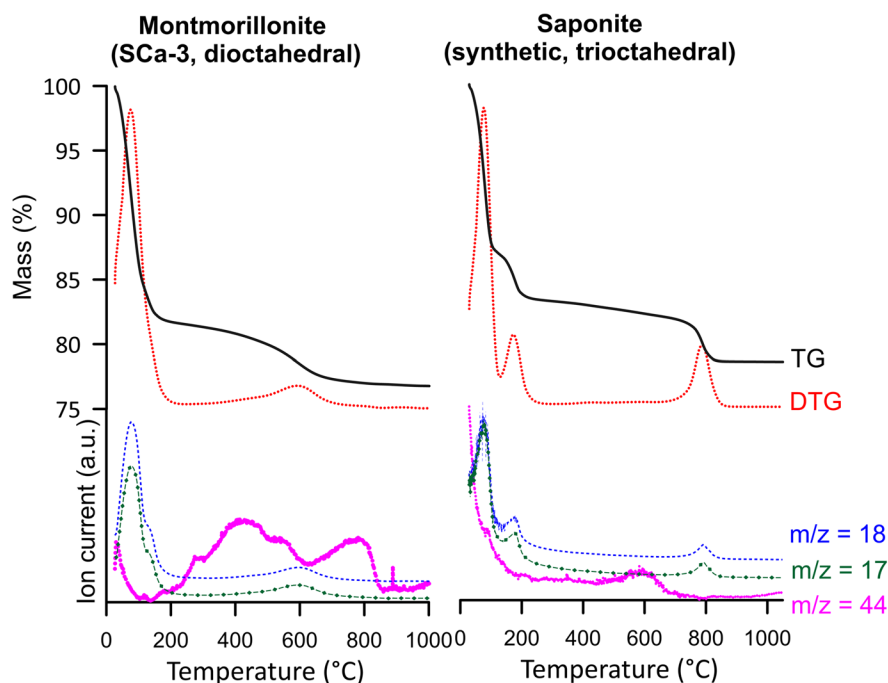

Fig. 1 An example of TGA and DTG curves of samples representing almost-pure dioctahedral (SCa-3 montmorillonite) and trioctahedral (high-charge synthetic saponite; Pelletier et al., 2003) smectites. The dehydration reaction at <200°C is followed by dehydroxylation above ~300°C, which are shown in the corresponding MS signal of H_2O (m/z = 18 and 17). Thermal removal of carboxyl groups from organic impurities and the decomposition of carbonate impurities are demonstrated by the CO_2 (m/z = 44) signal below 500°C and above 600°C, respectively. The analysis was performed under dry N_2 at a flow of 100 mL/min, with a constant heating rate of 20°C/min. Ion currents not to scale. *Note:* All natural smectite samples shown here and in the following figures come from the Source Clays Repository of The Clay Minerals Society. Unless specified otherwise, all thermal analyses presented in this paper were performed using a TA Discovery TGA (USA) instrument and ThermoStar GDS 320 MS from Pfeiffer (Göttingen, Germany); ~20 mg of loosely packed powder, using a wide 50 μL Platinum HT sample pan without a lid

of smectites with adsorbed organic compounds is a field in and of itself with dedicated reviews (e.g. Xi et al., 2005; Plante et al., 2009; Yariv et al., 2011).

Among many thermal analysis methods (see Emmerich, 2010), a few have been used widely for smectites and related clay minerals, and are the most meaningful for their characterization: thermogravimetric analysis (TGA), differential thermal analysis (DTA), and its modern successor – differential scanning calorimetry (DSC). If a sample is analyzed simultaneously using more than one of the techniques (e.g. TGA and DTA), such a mode of analysis is often referred to as Simultaneous Thermal Analysis (STA). The evolved gas analysis (EGA), which allows determination of the composition of gases and vapors evolved from a sample during heating in a TGA or DTA/DSC analyzer, is a form of STA. Among the different means of analyzing gas evolved from clay samples, infrared spectroscopy (IR) and mass spectrometry (MS; also coupled with gas chromatography – GC-MS) are the most commonly used.

Thermogravimetric analysis presents weight change with temperature or time. In most cases this corresponds to the extent of a clay's weight loss (in mg or weight %) during heating in an inert gas atmosphere, such as N_2, Ar, or He. However, under specific circumstances, mass gain can occur during TGA experiments, i.e. when an oxidizing agent or water molecules are present in the sample's environment. Common practice when reporting TGA results is to present a first derivative of the original mass change curve over time or temperature. Such a derivative is referred to as the DTG curve. Differential thermal analysis returns the temperature difference between the sample and an inert reference material under the same heating conditions. Similar to DTA, DSC measures the heat flow ($J K^{-1} mol^{-1}$) needed to maintain the same temperature of the sample and the inert reference material, which enables the heat capacity to be obtained (Giese, 1990). All the methods mentioned require some kind of purge gas which, in general, is meant to remove the thermal reaction products. A moisture analyzer is a low-temperature alternative to the TGA instrument, capable of measuring weight change (usually due to dehydration) from room temperature typically up to 200 or 250°C, with no purge gas flow.

Any thermal analysis can be performed in two modes depending on the rate of heating: (1)

isothermal – temperature is increased quickly to the desired value and kept constant for the remaining part of the experiment; (2) non-isothermal – temperature varies during the experiment. This mode is represented by, for example, heating or cooling with a constant rate to the final temperature. The most common way of performing thermal analysis is to use a predefined (isothermal or non-isothermal) temperature program. Controlled-rate thermal analysis (CRTA) is a specific case of non-isothermal or quasi-isothermal conditions in modern TGA instruments, where the sample's reaction rate (e.g. weight loss per time) is set as constant, but the heating rate varies (Ding & Frost, 2002; Rouquerol et al., 2013). As the temperature controller keeps the reaction rate constant during CRTA, temperature change with time for a particular experiment is not known beforehand. Whereas DTA and DSC usually need the linear heating/cooling mode (with exceptions, see Boller et al., 1994), TGA can operate in any isothermal or non-isothermal mode, or a combination of both.

Measurement Accuracy and Precision

Thermal-reaction temperatures are commonly reported based on the position of the corresponding DTG or DTA peak. A number of factors affect the position of the peak, which can hamper straightforward comparisons among reaction temperatures reported in various studies (Emmerich, 2010). First, a positive correlation occurs between the DTG or DTA peak temperatures and the heating rate in non-isothermal conditions due to kinetic effects. Second, the peak temperature is dependent on the particular thermal analyzer's temperature calibration, which should be based on at least two points in the range corresponding to the tested reaction. Curie temperature reference materials are commonly used for TGA instruments, whereas temperature and enthalpy of fusion are used in DTA and DSC instruments (Della Gatta et al., 2006). Theoretically, ~1 K (1°C) should be considered as a standard error in the thermal analysis of smectite in well-calibrated instruments. In practice, however, several factors may cause the actual sample temperature to deviate from the measured value even more (see Emmerich, 2010 for comprehensive review). As a result of a poorly crystalline structure, heterogeneous cation distribution, the particularly small size of its crystallites (both planar and crystallite thickness),

and their diverse means of agglomeration, smectite samples do not return sharp, well-defined thermal events. These features, along with operator-dependent choices during data mathematical processing, all result in the real accuracy and precision of determining reaction temperature being in the range of a few °C.

Accuracy of the mass-loss measurement can be tested using a homogeneous material with a well-constrained mass loss in a given temperature interval, such as Ca-oxalate monohydrate (Bish & Duffy, 1990; Plante et al., 2009). Thermal drift (i.e. the profile of mass or heat flow change with temperature in the absence of any reactive material) should be measured for each thermal analysis instrument and a mode of analysis. Thermal drift can be determined on an empty pan or an unreactive sample with a well-calibrated instrument under conditions corresponding to the experimental sample analysis and the test results should be applied to correct an experimental sample curve. A well-calibrated TGA instrument and method should return the mass-loss precision in the range of 0.1%.

Thermal Reactions of Smectites

Dehydration

Dehydration is the loss of molecular water (H_2O) adsorbed on or within clay-mineral particles. Upon drying, H_2O molecules are removed sequentially following the strength of their interactions with the smectite surface. The entire physisorbed water condensed in meso- and micropores of particles is removed at room temperature under the flow of dry purge gas. Bulk (bound via H-bonds to other H_2O molecules) smectite interlayer water is in equilibrium with the external moisture and, therefore, it is removed along with the physisorbed water albeit at a lower rate (Emmerich et al., 2018; Ferrage et al., 2010; Salles et al., 2009). Therefore, distinction between the bulk interlayer and the external, physisorbed water is hardly possible in thermal analysis as no temperature–time cutoffs are applicable. The removal of physisorbed and bulk interlayer water is completed much below 100°C. Due to the difference in solidification and fusion temperatures of physisorbed water, the DSC-based thermoporometry

(freezing conditions, below 0°C) is the best temperature-differentiation method that can be applied to address the distinction between total interlayer and micropore capillary water (Grekov et al., 2019; Salles et al., 2010).

In a fully hydrated smectite, some water molecules form a hydration shell around the smectite's interlayer cations. Once the bulk interlayer water is removed during dehydration, the remaining H_2O molecules become organized around the interlayer cations in a fashion and number dependent on the cation's hydration energy (Salles et al., 2015), expressed as the cation's hydration enthalpy (Table 1). The larger the absolute value of the cation hydration enthalpy (see Table 1 for an explanation of ΔH^o), the lower the probability for the cation to bind directly to the smectite's siloxane surface, the stronger the interaction between water molecules and the interlayer cation, and, therefore, the greater the energy that is required to remove any remaining strongly bound water (Webb et al., 1986).

The cation's hydration enthalpy is reflected by the pattern of smectite dehydration. Except for Li^+-saturated smectites, the interlayer's monovalent cations produce a single DTG dehydration peak below 100°C, whereas two DTG peaks or a high-temperature shoulder (up to ~200°C) usually correspond to high-enthalpy cations (polyvalent and Li^+; Fig. 2; El-Barawy et al., 1986). The fewer the H_2O molecules around interlayer cations, the greater the activation energy (E_a) of dehydration and the higher the temperature needed to remove the remaining H_2O. In extreme cases, H_2O dissociation leads to the hydrolysis of interlayer cations by OH that can remain in the smectite interlayer, even up to 500°C, which affects the course of dehydroxylation (Kuligiewicz & Derkowski, 2017).
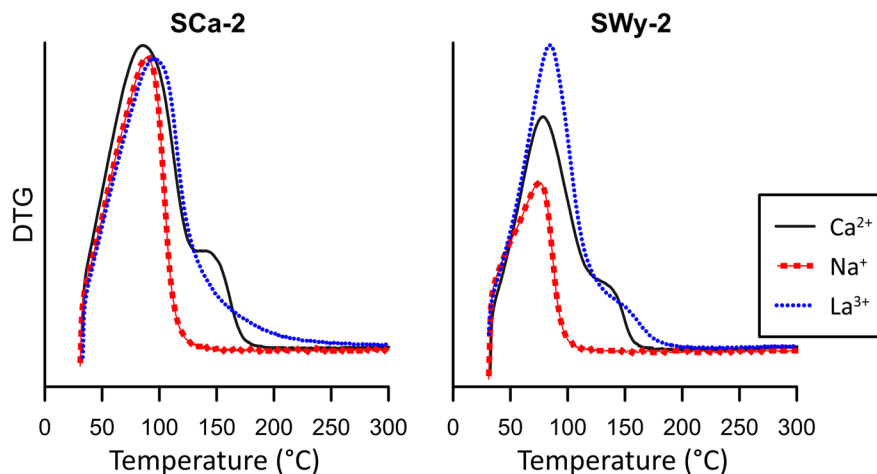
NH_4^+-exchanged smectites show very low mass loss due to dehydration as the ammonium cation has a low hydration enthalpy (Table 1); however, the smectite undergoes an exothermic deammonization reaction at 300–400°C resulting in weight loss and leaving smectite in H^+ form (Mackenzie & Bishui, 1958; Seiffarth & Kaps, 2009).

Unless a sample contains an impurity that provides mass loss at low temperature (<200°C, e.g. gypsum, zeolites, halloysite, and soil organic matter; see the Impurities section below), the quantity of H_2O removed from a clay during thermal

Table 1 The hydration enthalpy ($-\Delta H^o$) after Smith ([1977]) and effective ionic radii for a given coordination number of inorganic cations commonly occurring in smectite interlayers in natural conditions and used in laboratory experiments, after Shannon ([1976])

Monovalent cations			Divalent cations			Trivalent cations		
Cation	$-\Delta H^o$ (kJ/mol)	Ionic radius (Å) for coordination number	Cation	$-\Delta H^o$ (kJ/mol)	Ionic radius (Å) for coordination number	Cation	$-\Delta H^o$ (kJ/mol)	Ionic radius (Å) for coordination number
H^+	1091	0.38 (I)	Mg^{2+}	1921	0.72 (VI) 0.89 (VIII)	Al^{3+}	4665	0.535 (VI)
Li^+	519	0.76 (VI) 0.92 (VIII)	Ca^{2+}	1577	1.00 (VI) 1.12 (VIII)	Cr^{3+}	4560	0.615 (VI)
Na^+	409	1.02 (VI) 1.18 (VIII)	Mn^{2+}	1841	0.67 (VI) 0.96 (VIII)	Mn^{3+}	4544	0.645 (VI)
K^+	322	1.38 (VI) 1.51 (VIII)	Fe^{2+}	1946	0.78 (VI) 0.92 (VIII)	Fe^{3+}	4430	0.645 (VI) 0.78 (VIII)
Cs^+	264	1.67 (VI) 1.74 (VIII)	Ni^{2+}	2105	0.69 (VI)	Co^{3+}	4651	0.545 (VI)
$NH_4^{+\,*}$	307	1.48 (VI) 1.54 (VIII)	Cu^{2+}	2100	0.73 (VI)	La^{3+}	3296	1.032 (VI) 1.160 (VIII)
			Zn^{2+}	2046	0.74 (VI) 0.90 (VIII)			
			Sr^{2+}	1443	1.18 (VI) 1.26 (VIII)			
			Ba^{2+}	1305	1.35 (VI) 1.42 (VIII)			

[*] After Sidey ([2016])

Fig. 2 DTG curves in the temperature range corresponding to the dehydration of Na^+-, Ca^{2+}-, and La^{3+}-exchanged montmorillonites. The analysis was performed under dry N_2 at a flow of 50 mL/min, with a constant heating rate of 5°C/min

dehydration corresponds to the smectite content in a sample (both as a discrete mineral and as a fraction of smectite-interstratified phases), and also depends on the hydration enthalpy of the interlayer cation, and – to a minor extent – the smectite layer charge (Środoń & McCarty, [2008]; Środoń et al., [2009]; Webb et al., [1986]). If used for a semi-quantitative estimation of smectite content, a sample needs to be

pre-equilibrated at a selected relative humidity (RH) that produces a particular degree of interlayer H_2O filling, the latter also being dependent on the interlayer cation type (Berend et al., 1995; Cases et al., 1997). Despite this ambiguity, the measured fraction of mass loss due to dehydration is good enough for a relative comparison among samples tested. For example, pure Ca^{2+}-saturated smectite equilibrated at ~50% RH contains ~16.5 wt.% of H_2O (as determined by drying at 200°C; Środoń & McCarty, 2008); the corresponding mass loss upon dehydration decreases proportionally to illite interstratification in illite-smectite (Środoń et al., 2009) and smectite mineral content in a sample (Środoń, 2009). When equilibrated at ~50% RH, dehydration would correspond to 6% mass loss in K^+-saturated smectite, ~10% in Na^+- and Li^+-saturated smectite, and almost 20% in Mg^{2+}-saturated smectite (Berend et al., 1995; Cases et al., 1997). The above-mentioned semi-quantitative measurement should not be carried out under any dry gas purge (common in TG instruments) as it triggers dehydration during the sample-weight stabilization under dry gas flow; a moisture analyser is thus preferred (Środoń et al., 2009).

Dehydroxylation

Dehydroxylation is the major thermal reaction of smectites and other 2:1 layer type clay minerals. It occurs between ~300 and 900°C and results in the extraction of a H_2O molecule formed by two adjacent OH groups and leaves one residual oxygen atom (O_r) in the structure:

$$2n(OH)^- = nH_2O \uparrow + nO_r^{2-} \tag{1}$$
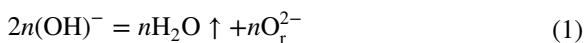
where n is the number of water molecules eliminated during dehydroxylation.

The actual thermogravimetric manifestation of the reaction is the loss of H_2O after its migration through the interlayer and out of the crystallite. The theoretical mass loss upon dehydroxylation is calculated as the molecular weight of H_2O per a smectite's formula unit molecular weight. Dehydroxylation produces an evolved gas pattern of H_2O exactly following the DTG curve and TG mass loss, corresponding quantitatively to Eq. 1 (Fig. 1). In Ca^{2+}- or Na^+-exchanged Fe-poor smectites mass loss corresponding to dehydroxylation is 4.7–4.9%, whereas

in nontronite it can be as low as 4.3%. Exchanging a smectite with a heavy cation such as Cs^+ can decrease the theoretical mass loss significantly. The smectite's mass loss due exclusively to dehydroxylation may not be clearly distinguishable in TGA analysis, and thus, may not correspond to the theoretical value. In numerous dioctahedral smectites, especially those having an interlayer cation of high hydration enthalpy (Ca^{2+}, Mg^{2+}, etc.), the onset of dehydroxylation overlaps with the dehydration of residual, strongly bound water (Bray & Redfern, 2000; Kuligiewicz & Derkowski, 2017).

The first control on the temperature of dehydroxylation is the octahedral occupancy. In dioctahedral 2:1 layer phyllosilicates the proton from one OH group migrates either along the shared edge of the octahedron or jumps across the octahedral vacancy to join the adjacent OH group (Guggenheim et al., 1987; Ogloza & Malhotra, 1989; Muñoz-Santiburcio et al., 2016). In dioctahedral smectites, dehydroxylation transforms the octahedral structural arrangement into a five-fold coordinated bipyramidal structure and the previously octahedral cations remain in a similar arrangement to the pristine structure (for details see Drits et al., 1995). The 2:1 layer thus remains at least partially intact. In the case of trioctahedral phyllosilicates, due to the lack of an octahedral vacancy where the residual oxygen could reside, OH groups cannot be removed without a reconstruction of the octahedral sheet; their dehydroxylation is accompanied by recrystallization and occurs at higher temperatures than in dioctahedral species, therefore (Fig. 1). The high-temperature DTG peak (usually >700°C) can serve as a distinction between trioctahedral layers or domains and dioctahedral counterparts in natural smectites. Synthetic saponites, however, showed strong dependence of the dehydroxylation temperature on the octahedral sheet cation composition: $Mg > Ni > Co > Zn$ (Vogels et al., 2005). Vogels et al. (2005) proposed that the smaller the octahedral cations, the greater the corrugation of the tetrahedral sheet, which results in greater thermal stability.

For dioctahedral smectites, the next factor controlling the temperature of dehydroxylation is octahedral symmetry. Drits et al. (1995, 1998) showed that the *cis*-vacant (*cv*) structure has a significantly higher dehydroxylation temperature (>600°C) than the *trans*-vacant (*tv*) layer structure (<600°C; Fig. 3). Those authors assigned that difference to the longer distance between non-shared OH edges in the
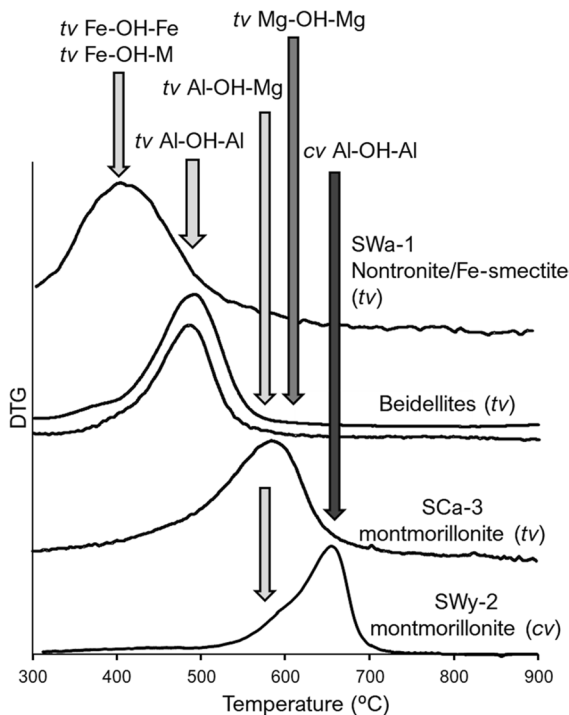
Fig. 3 DTG curves showing the difference in dehydroxylation of *trans*-vacant (*tv*) and *cis*-vacant (*cv*) dioctahedral smectites along their dominating octahedral cation-OH composition (after Derkowski et al., 2012a). Analysis preformed under dry N_2 at 50 mL/min flow, with a constant heating rate of 5°C/min

cv structure than the shared OH edge of the octahedron in the *tv* coordination, resulting in the less probable and longer H^+ jump between the OH groups in the *cv* coordination. Besides, in contrast to one-step dehydroxylation of *tv* layers, dehydroxylation of aluminous *cv* smectite is a two-step process that involves the Al cation migration to *cis*-sites and results in the pseudo-*tv* structure of the dehydroxylate (Drits et al., 1995; Stackhouse et al., 2004), the same as that of the dehydroxylated pristine *tv* smectite. In *tv* Mg-Fe-rich smectites (e.g. nontronite), however, some cations migrate to *trans*-positions during dehydroxylation in order to redistribute the Fe–O bonds, resulting in a *cv* dehydroxylated structure (Muller et al., 2010a, b Drits & Zviagin, 2009).

Following Drits et al. (1998), Wolters and Emmerich (2007) and Emmerich et al. (2009) adopted 600°C as the dehydroxylation temperature boundary and suggested using it for the determination of *cv* and *tv* compounds in smectites.

A broad temperature range of dehydroxylation is observed for all dioctahedral clay minerals, including smectites. Guggenheim et al. (1987) and Guggenheim (1990) explained this effect as a continuous recombination of bonds between the remaining OH and octahedral cations in a progressively dehydroxylated 2:1 layer. Drits et al. (2012a,b) and Derkowski et al. (2012a) suggested that the reaction model is homogeneous; the 2:1 layers are only either non-dehydroxylated or completely dehydroxylated, but the temperature of maximum dehydroxylation as well as the temperature range of dehydroxylation are controlled by the bond strength between OH groups and octahedral cations, i.e. the octahedral sheet composition (Drits et al., 2012b) and the crystallite thickness distribution (see also Pérez-Maqueda et al., 2004, Perez-Rodriguez et al., 2010). The latter is not applicable to smectites due to their ultrafine planar size and small crystallite thickness. The relative order of dehydroxylation temperature for *tv* dioctahedral smectites can be expressed by the following sequence (Derkowski et al., 2012a), (Fig. 3):

$$Mg - OH - Mg > Al - OH - Mg$$
$$> Al - OH - Al > Al - OH - Fe$$
$$> Fe - OH - Fe$$
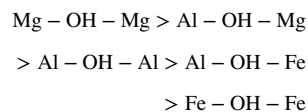
which is supported by the quantum mechanical calculations. The order of dehydroxylation temperature is controlled by the octahedral cation–OH bond strength, thus O…H distance (Molina-Montes et al., 2008; Botella et al., 2004). Although 300°C is applied commonly as the lowest temperature boundary of dehydroxylation (Fig. 3), long isothermal treatment provides energy sufficient to shift the onset of reaction to <300°C in the *tv* Fe-OH-Fe environment, i.e. nontronite (Środoń & McCarty, 2008; Kuligiewicz & Derkowski, 2017).

Heterogeneity of the octahedral sheet's cation composition contributes to the broad range of smectite dehydroxylation temperature; in smectite that has one cation species dominating the octahedral sheets the temperature range of dehydroxylation is narrower than those observed in smectites with heterogeneous octahedral composition (Drits et al., 2012a). In trioctahedral smectites the octahedral sheet is rarely fully occupied by cations. Locally occurring vacancies, e.g. in stevensite, produce dioctahedral domains

which dehydroxylate at temperatures corresponding to the dioctahedral smectite (i.e. montmorillonite).

The interlayer cations' hydration enthalpy controls the temperature of final dehydration and, thus, the degree of overlap for the dehydration and dehydroxylation reactions in some dioctahedral smectites (Kuligiewicz & Derkowski, 2017; Fig. 4). Also, the interlayer cation size and its potential for migration into the octahedral sheet play a role in the pathway of smectite dehydroxylation. Early DTA studies demonstrated that the interlayer cation influences the temperature of maximum dehydroxylation (El-Barawy et al., 1986; Mackenzie & Bishui, 1958). Later, Bray and Redfern (2000) and Kuligiewicz and Derkowski (2017) found differences in the kinetics of the dehydroxylation reaction in a smectite containing monovalent and divalent interlayer cations. Cs^+ is the largest inorganic cation that can pillar the interlayer (Table 1), allowing H_2O molecules generated during dehydroxylation to diffuse easily, resulting in a decrease in the temperature of dehydroxylation in dioctahedral smectites (Fig. 4). The more beidellitic the smectite structure is, the greater the effect of Cs^+-pillaring (Fig. 4: beidellite > beidellitic montmorillonite and nontronite > montmorillonite) because of the repulsion forces between adjacent siloxane surfaces created by Al substitution in the tetrahedral sheet and also the potential for the Cs^+ cation to be located above the Al-substituted tetrahedra instead of the ditrigonal cavity (Cuadros, 2002; Ngouana & Kalinichev, 2014). The cation size, however, seems to result in an opposite trend in trioctahedral smectites; the larger the interlayer cation, the higher the temperature of dehydroxylation (Fig. 4). The ability to block efficiently the ditrigonal cavity by a large cation, which suppresses H^+ migration into the adjacent OH group, is likely the reason for this effect.

In montmorillonites, where layer charge is generated in the octahedral sheet, dehydration enables small cations to migrate into the ditrigonal cavity of
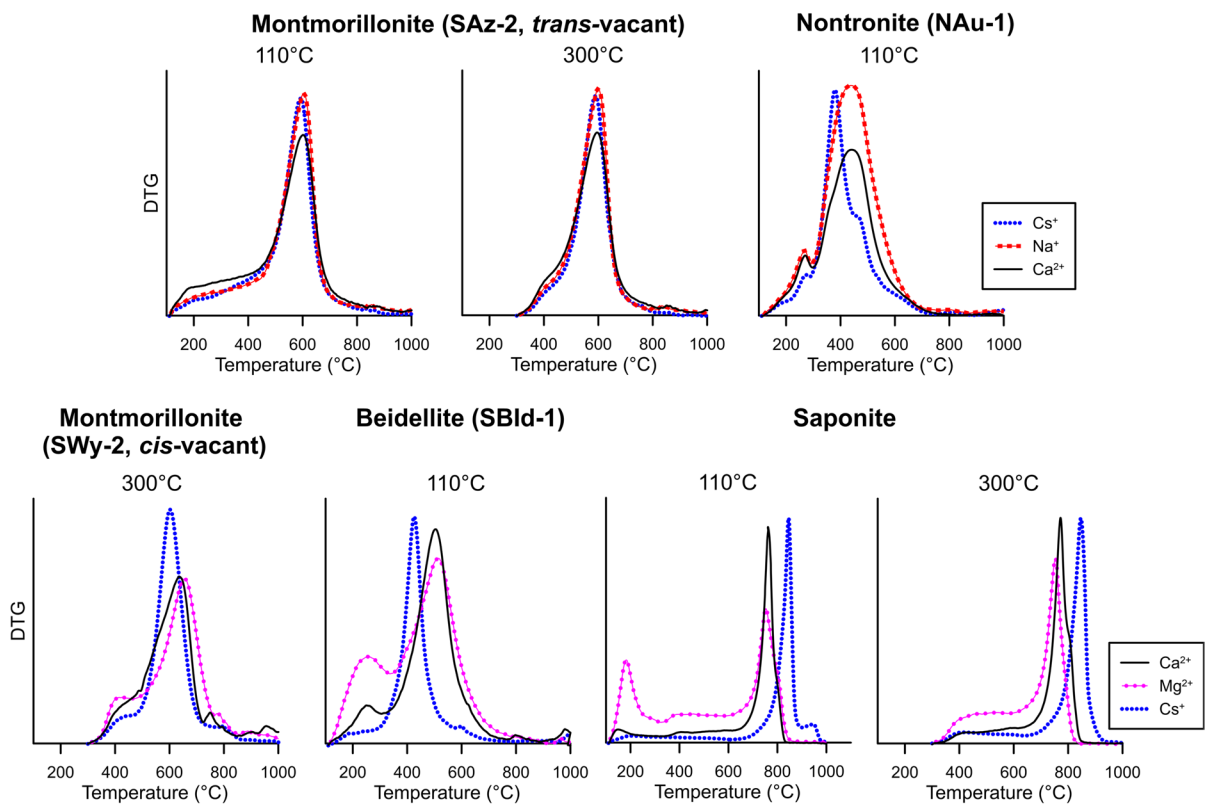

Fig. 4 DTG curves of smectite reference samples saturated with various inorganic cations. The analysis was performed under a 100 mL/min flow of dry N_2, with 4 h isothermal heating at the temperatures indicated on the figures, followed by heating to 1000°C at a constant rate of 5°C/min

the tetrahedral sheet and even further into the octahedral vacancy, forming pseudo-trioctahedral domains (Emmerich et al., 1999; Hofmann & Klemen, 1950; Komadel et al., 2005, and references therein; Skoubris et al., 2013). The Hofmann-Klemen effect affects the pattern of dehydroxylation, forming an additional DTG peak at temperatures corresponding to trioctahedral domains. Not only Li^+, commonly used in reducing layer charge, but also other small cations can produce such thermal effects. Koster van Groos and Guggenheim (1989) explained differences observed between the dehydroxylation of Mg^{2+}- and Ca^{2+}-exchanged montmorillonite as resulting from the different abilities of Mg^{2+} and Ca^{2+} to migrate toward the residual oxygen during the dehydroxylation reaction. The ability to form pseudo-trioctahedral domains must then depend on the kinetics of dehydration and small-cation migration through the ditrigonal cavity. Indeed, as presented in Fig. 5, Li^+ migration (Li^+ $-\Delta H^o = 519$ kJ/mol; Table 1) forms the high-temperature DTG peak weakly dependent on the dehydration temperature prior to dehydroxylation, whereas Mg^{2+}-montmorillonite (Mg^{2+} $-\Delta H^o = 1921$ kJ/mol; Table 1) produces a pseudo-trioctahedral DTG signature at ~900°C, which is

proportional to the temperature and time of isothermal dehydration (Fig. 5). Fast dehydroxylation during ramp-heating itself may not be sufficient to quickly and completely dehydrate Mg^{2+} and fix the cation in the ditrigonal cavity or the octahedral sheet.

Dehydrogenation

Dehydrogenation proceeds during thermal treatment of Fe(II)-bearing phyllosilicates, resulting in the removal of one hydrogen atom while simultaneously oxidizing one Fe(II) cation that is octahedrally coordinated with the OH group (Farmer et al. 1971; MacKenzie & Berezowski, 1984; Rancourt et al., 2001; Sanz et al., 1983; Wicks & Ramik, 1990).

In vacuum and in an inert gas atmosphere, the dehydrogenation reaction proceeds as follows:

$$2(Fe^{2+} + OH^-) \rightarrow 2(Fe^{3+} + O_r^{2-}) + H_2 \uparrow \qquad (2)$$
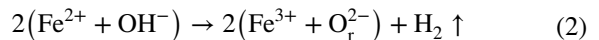
resulting in the formation of H• radicals that evolve from a sample as H_2 gas, which can be recorded in an EGA mass spectroscopy signal as m/z = 2 (Lempart et al., 2020). The reaction proceeding via Eq. 2 produces negligible mass loss, 1/9 of that produced
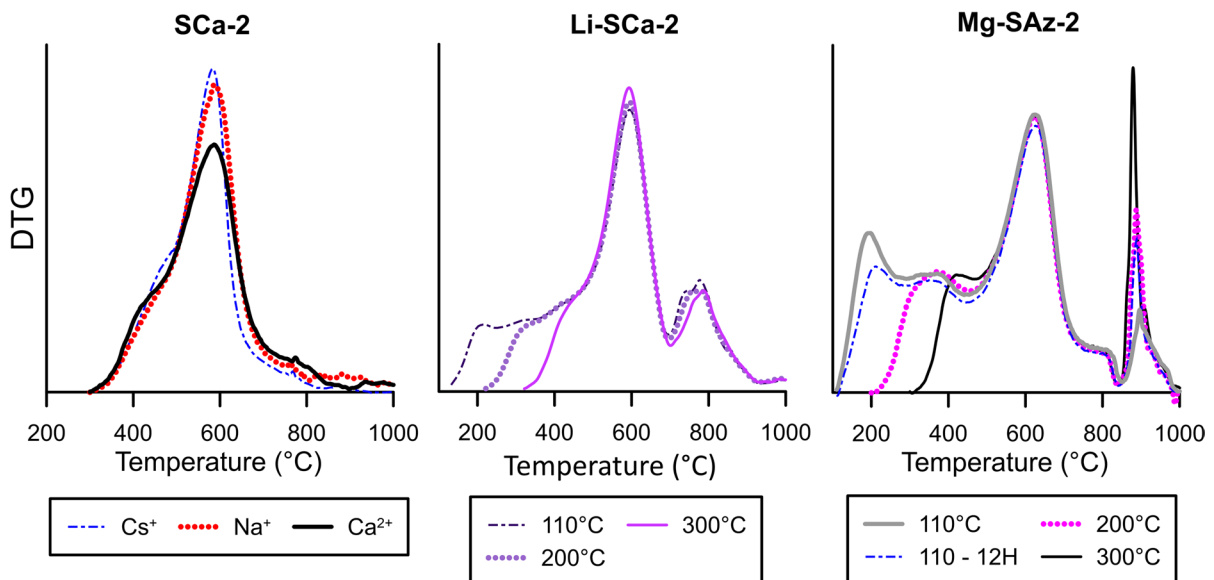

Fig. 5 The effect of cation migration into the octahedral sheet. DTG curves of Li^+-exchanged and Mg^{2+}-exchanged montmorillonites preheated isothermally under a flow of 100 mL/min of dry N_2 for 4 h at various temperatures (as stated in the legend) followed by heating to 1000°C at a constant rate of 5°C/min. The DTG curves of the SCa-2 sample saturated with other cations and preheated isothermally at 300°C are given as reference

by dehydroxylation (Eq. 1). Dehydrogenation usually overlaps with the temperature range corresponding to dehydroxylation, which has led to numerous incorrect interpretations of the reaction mechanisms and products (Heller-Kallai & Rozenson, 1980). Dehydrogenation removes the hydroxyl H, reducing the amount of OH groups available for dehydroxylation, which results in a weight loss that is much lower than the theoretical value for dehydroxylation. In contrast to what has been reported in the literature, Fe(II)-free phyllosilicates do not undergo dehydrogenation and do not produce H_2 under normal pressure (Heide & Földvari, 2006 cf. Lempart et al., 2020).

Under O_2-bearing gas (e.g. air), the reaction follows the same pathway as in Eq. 2, with H• radicals combined with ambient oxygen to produce H_2O.

$$2(Fe^{2+} + OH^-) + 1/2\ O_2 \rightarrow 2(Fe^{3+} + O_r^{2-}) + H_2O \uparrow \quad (3)$$
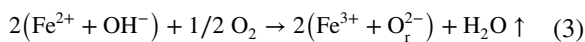
The presence of oxygen enhances dehydrogenation, shifting the reaction to lower temperatures. The MS curve of $m/z = 18$ of evolved gas in the reaction from Eq. 3 is excessive to the DTG curve, because H_2O is not produced within the heated crystallite and thus does not produce the corresponding weight loss (Lempart et al., 2020).

In contrast to Eq. 3, only a specific portion of structural Fe(II) can oxidize under O_2 (e.g. air) following the reaction:

$$2Fe^{2+} + \frac{1}{2}O_2 \rightarrow 2Fe^{3+} + O_r^{2-} \quad (4)$$
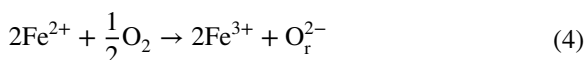
because the structural Fe(II) in a 2:1 layer is not readily available for binding with ambient oxygen and the reaction presented in Eq. 3 is preferred unless $^{VI}Fe(II)/OH$ ratio > 1. Such a reaction as in Eq. 4 is possible during or after the high-temperature recrystallization when Fe(II) is exposed to ambient O_2 (Lempart et al., 2018).

Because of structural constraints, Fe(II) in natural smectites occurs in numerous trioctahedral species (Kohyama et al., 1973; Stucki, 1988); therefore, these phases are the most prone to dehydrogenation. In nature, dehydrogenation may be responsible for the depletion of OH groups in so-called oxy-smectites (Dainyak et al., 1981). Dehydrogenation following Eq. 2 or Eq. 3 is expected upon heating Fe-reduced nontronites (Heller-Kallai, 1997a; Lear & Stucki, 1985).

In F-bearing smectites, usually trioctahedral and synthetic smectites (Christidis et al., 2018), defluorination occurs as F• radical loss above 500°C and HF loss above 850°C (Heller-Kallai 1997b; Wicks & Ramik, 1990).

Smectite Structural Transformation upon Heating

Amorphization and recrystallization are the reactions that occur during thermal destabilization of the dehydroxylation and dehydrogenation products (Grim & Rowland, 1942a,b; Meyers & Speyer, 2003). At temperatures higher than dehydroxylation, dioctahedral smectites undergo amorphization and then recrystallize into a topotaxic set of mullite, spinels, quartz or cristobalite, and pyroxenes (Bradley & Grim, 1951; Brett et al., 1970). The degree and temperature of amorphization and transformation depends on the octahedral-sheet composition. Beidellite dehydroxylate is the most stable high-temperature smectite phase, the irreversible amorphization of which has not been observed below 900°C (Derkowski et al., 2012a; Derkowski & Kuligiewicz, 2017; Kawano & Tomita, 1991b), whereas recrystallization occurs above 1200°C (Bradley & Grim, 1951). Sequentially heated Mg-rich dioctahedral smectites show an onset of amorphization at the end of dehydroxylation, whereas maximum amorphization is reached by ~800°C (Garg & Skibsted, 2014; Derkowski & Kuligiewicz, 2017), which provides their pozzolanic properties, but irreversibly removes their adsorption potential. In smectites rich in redox-active metals, i.e. nontronite, the temperature of transformation and the composition of transformation products depend heavily on the type of ambient gas (MacKenzie & Rogers, 1977).

In trioctahedral smectites, transformation proceeds along with dehydroxylation; after initial amorphization, a pyroxene-like structure and an olivine-like structure are formed (Vogels et al., 2005).

In contrast to dehydroxylation and dehydration, phase transformation is manifested in the DTA or DSC curves and not in TGA and TGA-MS, because it is not associated with a mass change or evolution of volatiles. However, note that at high temperature (>800°C), especially for isothermal experiments, some alkali cations can be removed due to vaporization, which may be responsible for occasionally

observed minor and slow weight loss over a broad temperature range.

Rehydration and Rehydroxylation

Rehydration is the adsorption of H_2O molecules by a dried material. Rehydroxylation is the reconstruction of the structural OH groups, i.e. reversal of the reaction in Eq. 1, in a dehydroxylated smectite structure that has not undergone phase transition (amorphization or recrystallization). Whereas rehydroxylation in general must be preceded by H_2O diffusion through the dehydroxylated structure, advanced rehydroxylation requires specifically the diffusion within the interlayer in order to access all potential reaction sites available in the 2:1 layer. Both rehydration and rehydroxylation can be observed in situ as mass gain once wet gas is delivered directly to the TGA chamber (Derkowski & Kuligiewicz, 2017). When exposed to air, dried smectite having divalent cations in the interlayer starts resorbing H_2O from ambient moisture within seconds (Fig. 6; Kanik et al., 2022). For this reason, in practice, smectite material for rehydration and rehydroxylation tests also needs to be pre-dehydrated or pre-dehydroxylated in situ. The rate and extent of rehydration in pristine, dried (i.e. dried below the temperature of dehydroxylation) smectite depends heavily on the pre-drying conditions and, thus, the extent of interlayer cation fixation, and
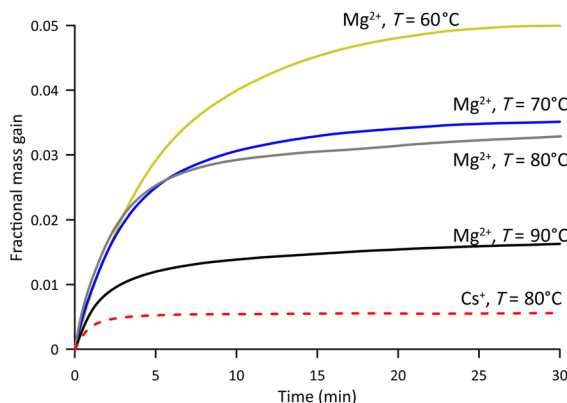

Fig. 6 Rehydration of a smectite reference sample (SWy-3), saturated with cations of contrasting hydration enthalpy, at various temperatures, after prior in situ drying for 4 h at 200°C. Mass gain is shown as fractional mass gain at a constant H_2O content of 9 g/kg air (not constant RH), normalized to the sample mass after drying at 200°C

the temperature and RH during rehydration (Fig. 6; Derkowski et al., 2012b, Gailhanou et al., 2017). Structurally, the extent of rehydration is controlled by the bonding between the siloxane surface and the interlayer cation; the greater the layer charge and the lower the cation hydration enthalpy, the stronger the bonding. K^+-exchanged high-layer charge smectites would not rehydrate extensively keeping their interlayer closed, whereas Ca^{2+}-exchanged smectite is prone to fast rehydration (Derkowski et al., 2012b; Kawano & Tomita, 1991a, b). Once a small interlayer cation, like Li^+ is dehydrated and migrates through the ditrigonal cavity in montmorillonite (Hofmann-Klemen effect; Fig. 5), however, the interlayer is fixed permanently, prohibiting rehydration (Derkowski & Kuligiewicz, 2017; Komadel et al., 2002). A similar effect occurs even if the interlayer cations do not migrate into the 2:1 layer: if layer charge is located in the octahedral sheet, dehydrated interlayer cations are bonded strongly to the 2:1 layer, resulting in rehydration slower than if the charge came from tetrahedral cation substitution (Kawano & Tomita, 1991a,b).

Rehydroxylation occurs mostly in the intact dehydroxylated phase that preserves the layer structure and can undergo the reverse of the Eq. 1 reaction (Derkowski et al., 2012a). Once smectite crystallites reach the high-temperature amorphization or recrystallization, the structural integrity is lost. Therefore, dehydroxylated trioctahedral smectite, Mg-rich montmorillonite, and nontronite do not have great potential for rehydroxylation, whereas beidellite is the most prone to rehydroxylation because its layer structure remains intact at high temperatures (Derkowski et al., 2012a).

Because dehydroxylation of originally *tv* and *cv* aluminum smectites produces a similar *tv* phase, when rehydroxylated it resembles a *tv* structure (Drits et al., 1995; Muller et al., 2000a, b). Indeed, when analyzed with thermal methods, such a rehydroxylated phase dehydroxylates at the temperature range typical for *tv* beidellite (<500°C; irrespective of the temperature of dehydroxylation of its pristine structure (Derkowski & Kuligiewicz, 2017; Fig. 7). A *tv* Fe,Mg-rich smectite that adopts a *cv* character after dehydroxylation can probably return to *tv* when rehydroxylated (Drits & Zviagina, 2009; Muller et al., 2000b). The most intense rehydroxylation occurs under H_2O vapor at temperatures of 250–350°C, even at extremely low H_2O activity. At such conditions,
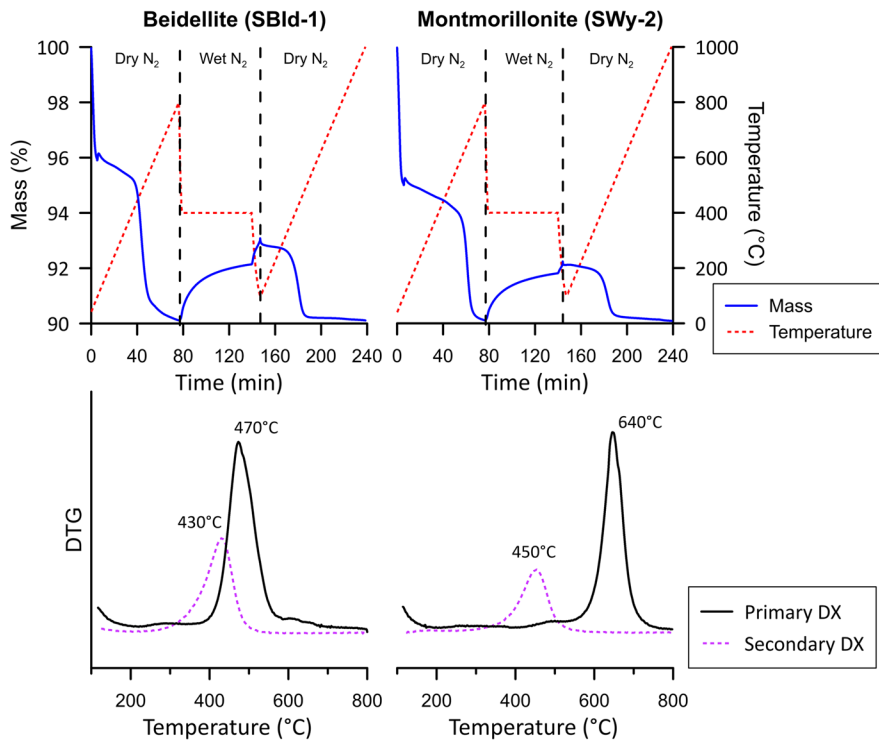
Fig. 7 An example of an in-situ experiment of an isothermal rehydroxylation reaction observed with TGA (after Derkowski & Kuligiewicz, 2017) on a Cs^+-exchanged beidellite (SBId-1) and montmorillonite (SWy-2). Note the initial dehydroxylation to 800°C under dry gas and switching to H_2O-rich gas for isothermal rehydroxylation, then secondary dehydroxylation to 1000°C under dry gas. The mass gain under wet gas corresponds to the rebuilding of OH groups

up to tens of % of the dehydroxylated dioctahedral smectite structure can be rehydroxylated within an hour of reaction (Fig. 7; Derkowski & Kuligiewicz, 2017). The mass gain observed during isothermal treatment of the prior dehydroxylated phase has been proven to correspond to true rehydroxylation by XRD and infrared spectroscopy (Kawano & Tomita, 1989, 1991b; Muller et al., 2000b; Derkowski et al., 2012a; Derkowski & Kuligiewicz, 2017). At reaction temperatures providing intense rehydroxylation, the interlayer's H_2O diffusion does not result in permanent rehydration (Derkowski et al., 2012b).

Rehydroxylation is site-specific and is influenced by several factors. If the layer charge is located in the tetrahedral sheet, the opening of the interlayer space during rehydroxylation is relatively easy due to large electrostatic repulsion between adjacent layers. Interlayer cation type also affects the rehydroxylation behavior of a smectite (Kawano & Tomita, 1989, 1991b; Emmerich et al., 2001; Derkowski et al., 2012a; Derkowski & Kuligiewicz, 2017). Interlayer

cations with relatively large radii (>0.13 nm in the eight-fold coordination; Shannon, 1976) act as pillars, which leads to a relatively large interlayer space of the dehydroxylate and enhances its rehydroxylation potential. Cations with large hydration potential also increase H_2O migration in the interlayer region, which is the prerequisite for further H_2O migration into the octahedral sheet and reformation of OH groups (Derkowski et al., 2012a,b). If an anhydrous cation has a small ionic radius (<0.08 nm, Li^+, Mg^{2+}), it can migrate into a pseudohexagonal cavity or into a vacant position of the former octahedral sheet and physically block access to the residual oxygen, which results in a reduced ability to rehydroxylate. Such cation migration results in irreversible collapse of the interlayer space (Emmerich, 2000; Emmerich et al., 2001; Derkowski et al., 2012a). In practice, rehydroxylation in smectites is controlled by the fraction of AlAlOH environment in the octahedral sheet, with no Al substitution in the neighboring tetrahedral sites ("pyrophyllite-like" domains), resulting in the lack of

charge-compensating interlayer cations blocking the ditrigonal cavity for H_2O migration. Another factor is the valence of the exchangeable cation – the greater the valence, the fewer cations are present in the interlayer space and the lower the chance of blocking the pathway of potential rehydroxylation (Derkowski et al., 2012a).

Experimental Factors Affecting the Results of Thermal Analysis of Smectites

Carrier Gas Composition and Pressure

Smectite thermal analysis is usually performed under dry gas purge in order to remove the products of dehydroxylation or dehydration. The presence of water vapor in the ambient gas changes the reaction pattern, shifting the reaction to higher temperatures following the H_2O content in the purge gas (Emmerich et al. 2017; Koster van Groos & Guggenheim, 1987, 1989; Levy & Hurst, 1993). Smectite dehydration and dehydroxylation reactions under high H_2O activity and high pressure were the subject of dedicated experiments enabling the prediction of smectite behavior under conditions relevant to geologic systems (Koster van Groos & Guggenheim, 1990, and references therein). Vacuum conditions decrease the smectite reaction temperatures with respect to ≥ 1 bar conditions (Wicks & Ramik, 1990).

An analysis of redox-sensitive minerals requires use of a virtually oxygen-free purge gas (Bottom, 2008, Bish & Duffy, 1990). The presence of oxygen in the purge gas can be tested in such cases using CuC_2O_4 (Lempart et al., 2018). The purge gas is considered virtually oxygen-free if no mass gain is detected during the experiment with pure CuC_2O_4.

Sample Form and Packing

With some exceptions, smectite samples are typically analyzed in a powder form. Before a thermal experiment, powdered samples should be homogenized and preferably sifted through a 100 or 200 μm mesh sieve, which allows for the reduction of the size of smectite aggregates present in the sample. In the case of montmorillonite that has a temperature of amorphization close to that of dehydroxylation, the presence of large aggregates leads to the formation of macroscopic
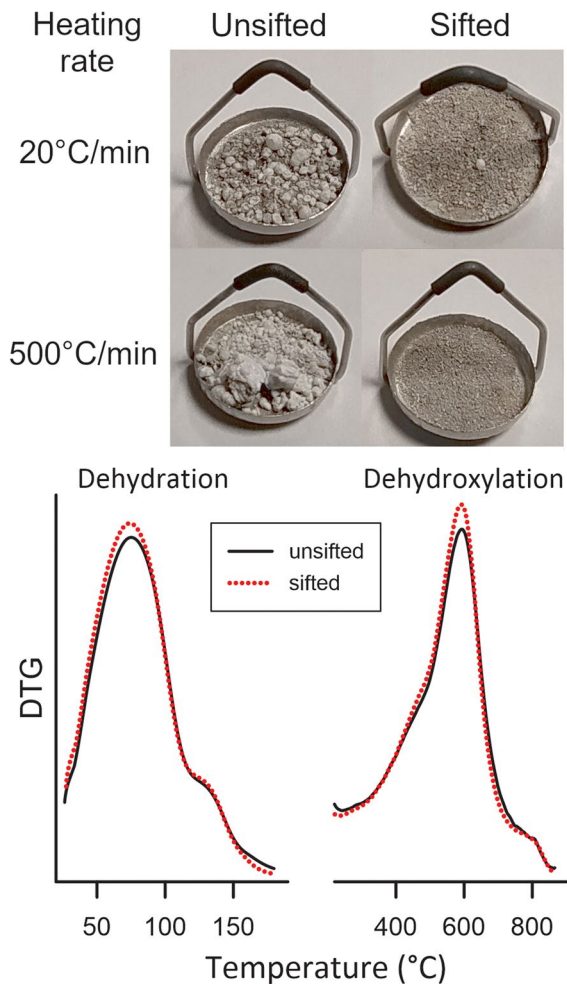

Fig. 8 The texture (upper) and DTG pattern (lower) of unsifted and sifted Ca^{2+}-exchanged montmorillonite sample (SCa-3) after heating to >1000°C at a constant rate of 20°C/min (DTG pattern) and 500°C/min under a flow of 50 mL/min dry N_2 gas

bubbles and hollow spheres, especially for samples with exchangeable cations of high hydration enthalpy, such as Ca^{2+}, Mg^{2+}, or Li^+ (Fig. 8; Emmerich, 2010; Emmerich et al., 2017). The spheres are probably produced by slow heat transfer inward and slow diffusion of H_2O outward from the aggregates. Interestingly, the formation of such spheres has virtually no effect on the DTG curve or mass loss during a TG experiment (Fig. 8).

The way powder is loaded into a holder can also affect the reaction temperature (Emmerich, 2010); a pressed sample delays the diffusion of the reaction volatile products out of the holder due to decreased

permeability. Although the effect is not greater than a few °C, and thus is within the temperature error (Schilling, 1990), use of a loose powder or exactly the same mode of pressing for all samples being compared is recommended. Also, the experiments involving surface reaction with ambient gas (i.e. dehydrogenation under oxidizing conditions) may be strongly affected by the sample permeability to gases.

The maximum reaction temperature correlates positively with the sample mass due to the heat capacity and the diffusion rate of volatile reaction products (Schilling, 1990; Wolters & Emmerich, 2007). However, as found by Derkowski and Kuligiewicz (unpublished data), up to 20% relative of smectite sample weight difference has a negligible effect on the reaction temperature and remains within the analytical error; 20% would thus be the maximum difference in the sample weights recommended for relative comparison. The greater the sample weight, the lower the relative influence of total measurement errors (weighing imprecision, thermal drift) that are usually expressed in absolute quantities, i.e. are independent of the sample size. However, upon heating, a smectite sample can change its bulk volume (due to recrystallization, amorphization) or electrostatic properties (due to dehydration, cation fixation), resulting in the holder overflow and the drop of a sample portion off the holder, which is detrimental to the analysis. Fortunately, a material drop is usually abrupt enough to be distinguishable from a slower thermal reaction

of smectites, allowing the results to be rejected from interpretation. Such a sample drop is typical for Li$^+$-montmorillonites at the temperature of dehydroxylation, when a sample is blown off the holder by purge gas (Fig. 9). Using a holder with a lid may prevent that problem (e.g. Emmerich et al., 2017; Wolters & Emmerich, 2007), but this would also induce a delay in removal of volatiles from the sample. The delayed removal of the reaction products by the gas purge results in momentary production of a water vapor atmosphere around the sample.

Factors Affecting Evolved Gas Analysis (EGA)

Isothermal reactions are usually not recorded in EGA. The EGA requires a high heating rate and high carrier gas flow, unless a vacuum system is used (Wicks & Ramik, 1990 cf. Lempart et al., 2020). High heating rates (and possibly large sample masses) are usually needed to keep the evolved gas in a concentration range that is easily determined by the applied spectrometric method.

In the MS signal, H_2O is represented by four spectral masses, the dominant m/z = 18, and the minor m/z = 17 (OH$^+$), whereas, the H_3O^+ (m/z = 19) and O$^+$ (m/z = 16) can be detected in orders of magnitude lower intensity (Meija et al., 2006; Emmerich, 2010). With pure dehydration and dehydroxylation reactions, the m/z 17 follows precisely m/z 18, and both signals
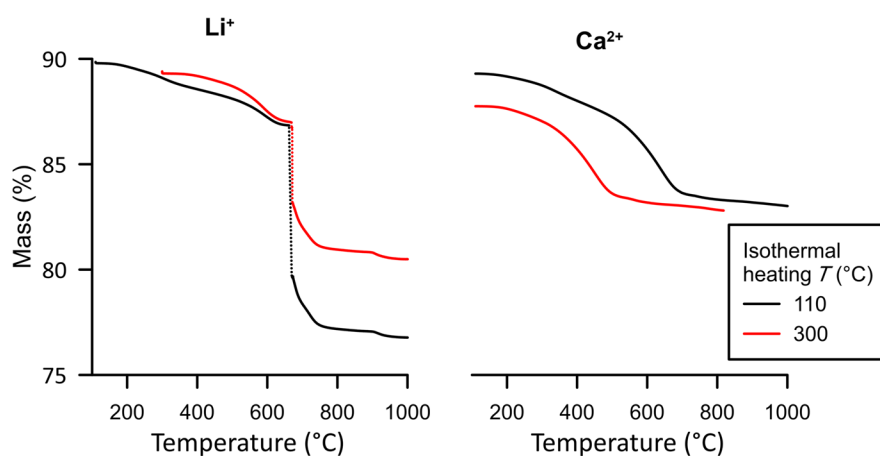

Fig. 9 TGA patterns of Li$^+$- and Ca^{2+}-exchanged montmorillonite (SWy-2) heated isothermally for 4 h at temperatures as indicated in the legend followed by ramp-heating at 10°C/min under a flow of 50 mL/min of dry N$_2$. Note the abrupt mass loss at almost the same temperature in Li$^+$-exchanged samples, originating from the sample dropping off the holder

overlap the DTG curve (Fig. 1). The NH_3 evolution from NH_4^+-smectites would produce excess m/z 17 whereas dehydrogenation under O_2 (or air) would produce an additional H_2O signal distinguishable as an excess to the DTG curve (Heller-Kallai, 1997b, Fig. 5 in Lempart et al., 2020; Fig. 1). Dehydrogenation that produces H_2 (m/z = 2) is difficult to detect and requires a fast sample-heating rate (≥20°C/min; Lempart et al., 2020) in MS or employing a GC–MS system.

Halogen elements present in trioctahedral smectites substituting OH groups (mostly F, also Cl, B) evolve from a smectite sample as hydrogen halides or radicals forming gaseous diatomic molecules (Heller-Kallai, 1997b; Wicks & Ramik, 1990). Strong reactivity of H-halide molecules with metals makes them react with any metal-based elements of the analyzer setup, however, and so ceramic pans and skimmer TGA-MS interfaces are suggested.

Impurities

The mass loss recorded with TGA in a pure smectite should correspond to the cation-dependent dehydration and the theoretical mass loss corresponding to dehydroxylation (Emmerich, 2010; Kuligiewicz & Derkowski, 2017). In nature, smectite never occurs as a pure mineral, even in bentonite beds. Also, even a thorough chemical treatment aimed at removing impurities and grain-size fractionation (Jackson, 1969), usually leaves some impurity in the studied smectite fraction. Some impurities are not reactive in the temperature range corresponding to major smectite reactions, e.g. the presence of quartz and feldspar only reduces the theoretical mass loss due to dehydroxylation. Other impurities, however, have their own thermal reactions that can strongly affect the thermal analysis pattern of smectite samples (Emmerich, 2010). The presence of discrete or interstratified kaolinite frequently coexisting with aluminous smectites (such as beidellites), increases the sample's mass loss in the dehydroxylation range, as kaolinite has three times more OH groups per formula unit to form H_2O than smectite. The above-mentioned impurities can be detected by XRD and for kaolinite also by infrared spectroscopy.

During smectite cation exchange with divalent cations, atmospheric CO_2 dissolved in the exchange solution binds with the cations forming carbonate impurities. In TGA tests they provide a significant mass loss corresponding to 44–52% of the carbonate content depending on the type of carbonate; the same mass loss would come from naturally occurring carbonate minerals present in a clayey sample (Emmerich & Smykatz-Kloss, 2002; Emmerich, 2010), if they were not carefully removed during the chemical pretreatment (Jackson, 1969). Therefore, even minute quantities of carbonate minerals, untraceable using other methods (e.g. XRD), can affect the smectite mass-loss determination. Thermal decarbonatization resulting in CO_2 evolved usually at temperatures of 700–900°C can be observed with EGA, however, e.g. by monitoring m/z = 44 in the TGA-MS setup (Fig. 1), in order to apply appropriate mass-loss corrections.

Sedimentary or soil organic matter (SOM) can be bound strongly to smectite surfaces and is difficult to remove even by extensive chemical treatment (Mikutta et al., 2005; Szymański et al., 2022). Thermal decomposition of recalcitrant SOM under neutral gas results in various evolved molecules, usually below 500°C, identifiable by EGA-MS as a series of various signals with m/z > 50 (Emmerich, 2010), along with those belonging to hydrocarbons (methane with m/z = 16), and CO_2 (m/z = 44; Fig. 1). The SOM-evolved H_2O (m/z = 18) and NH_3 (m/z = 17) overlap with the smectite-derived H_2O signal. Under neutral gas, only a portion of SOM decomposes, leaving charcoal as a high-temperature product. If run under oxidizing gas (i.e. air), SOM oxidizes completely, usually below 400°C, resulting in evolved H_2O and CO_2 identifiable by EGA, and the excess mass loss equal the SOM content. The difference in mass loss and evolved gas composition (especially CO_2) between the experiments under neutral and oxidizing gas can reveal the SOM presence. However, structural Fe(II) present in the smectite or associated phases can decrease mass loss under oxidizing conditions, canceling the SOM effect, leaving CO_2 (m/z = 44) as the most reliable proxy.

Hydrous sulfate minerals (e.g. gypsum) are the first to be removed during smectite sample pretreatment. However, if present in a sample even in minute amounts, their mass loss upon dehydration at 100–200°C (for example, 21% in gypsum) increases smectite dehydration. Desulfurization occurring at >700°C – in the range of trioctahedral smectite dehydroxylation – results in a loss of almost 50% of

gypsum mass, which can be detected easily using EGA-MS (m/z: 64, 48, 32; Emmerich, 2010; Dietel et al., 2017). If analyzed under oxidizing conditions, trace sulfides, e.g. pyrite, reacting with O_2 also release SO_2 albeit at lower temperatures (<500°C; Dietel et al., 2017). When reacting with H_2O coming from a smectite's dehydroxylation at 500–800°C, sulfides produce H_2S molecules (Levy & White, 1988).

Kinetic Calculations of Smectite Thermal Reactions

Theoretical Background

As in any other reaction, de- and re-hydration and de- and re-hydroxylation can be tracked using common kinetic approaches. The comprehensive review of methodology applicable in solid-state kinetics studies of thermally stimulated processes can be found elsewhere (e.g. Khawam & Flanagan, 2006a,b; Vyazovkin et al., 2011, 2020). A brief introduction of the key methodological points is presented below, with special emphasis on methods applicable to the thermal reactions of smectite.

The majority of methods in solid-state kinetic analysis of thermally stimulated reactions are based on the following equation:

$$\frac{d\alpha}{dt} = k(T)f(\alpha) \tag{5}$$

which states that the reaction rate ($d\alpha/dt$) is dependent on the absolute temperature (in K) through the reaction rate constant (k(T)) and on the extent of conversion (α) through the reaction mechanism ($f(\alpha)$). The extent of conversion is the dimensionless parameter describing progress of the reaction and is scaled between 0 and 1, where 0 corresponds to the start and 1 to the completion of the reaction. The extent of conversion must correspond to a change of some measurable property of a material that represents the reaction progress. In TGA practice, this parameter is mass change and α is expressed conveniently as the ratio of mass change at a given time during the reaction to the mass change corresponding to the completion of the reaction e.g. to full dehydroxylation. Calculating the reaction progress from DTA and DSC data requires prior integration of the peak over time or temperature. The reaction mechanism in Eq. 5 is a

function describing the progress of a reaction based on the molecular reaction mechanism and/or reactant geometry and can take various mathematical forms (Khawam & Flanagan, 2006a,b; Vyazovkin et al., 2011). The dependence of the reaction rate constant on temperature is most commonly expressed with the Arrhenius equation:

$$k(T) = A\exp\left(\frac{-E_a}{RT}\right) \tag{6}$$

where A is the pre-exponential factor, E_a is the activation energy, and R is the gas constant.

Substituting Eq. 6 into Eq. 5 gives:

$$\frac{d\alpha}{dt} = A\exp\left(-\frac{E_a}{RT}\right)f(\alpha) \tag{7}$$

or in the logarithmic form:

$$\ln\left(\frac{d\alpha}{dt}\right) = \ln A + \ln(f(\alpha)) - \frac{E_a}{RT} \tag{8}$$

Finding the triplet $f(\alpha)$, E_a, and A allows for the full kinetic description of the reaction studied. However, many kinetic studies present only an estimation of E_a as the most relevant reaction-specific parameter. Depending on the mode in which the thermal analysis experiment was performed, E_a can be calculated using isothermal or non-isothermal data, the latter most commonly coming from linear
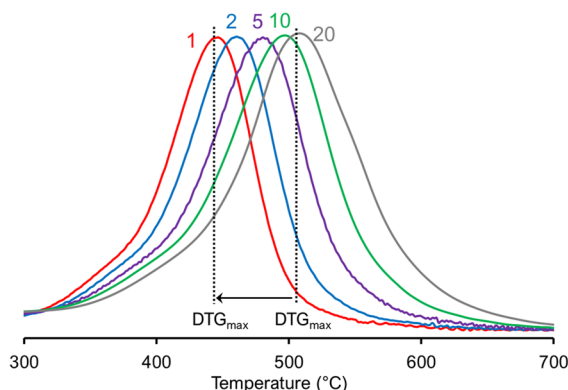

Fig. 10 The examples of linear, ramp-heating of a Na^+-beidellite sample to 1000°C under a 50 mL/min flow of dry N_2 and at various heating rates. The rates are indicated at the DTG peak in °C/min. The shift between the DTG_{max} peaks can be used to determine the activation energy of dehydroxylation

heating experiments (Fig. 10). In any case, using at least three temperature programs is strongly advised (Vyazovkin et al., 2011; Figs. 10, 11b), and at least five points are required to detect any non-Arrhenius behavior of the reaction, which manifests itself by non-linearity of Eqs. 6 and 8 (Vyazovkin et al., 2020).

Two general types of kinetic calculations are used for thermal analysis data. The model-fitting approach is based on fitting one of the reaction models available in the literature to Eq. 5 or its integral form and finding the best-fitting model, simply by comparing its linearity with experimental data. The reaction mechanism may or may not include adjustable parameters, which can later be interpreted in terms of a rate-controlling model (Bray & Redfern, 2000; Giese, 1990; Vyazovkin et al., 2011). In smectites, the isothermal model-fitting approach has been proved useful for determining the kinetics of dehydration (Bray & Redfern, 1999), dehydroxylation (Bray & Redfern, 2000), and rehydroxylation (Derkowski & Kuligiewicz, 2017).

The second type of calculations are those using the isoconversional methods (Criado et al., 2008, Perez-Rodriguez et al., 2010; Vyazovkin, 2015, Vyazovkin, 2021), in which E_a and A are calculated without any assumptions of a particular kinetic model or the reaction order. The basic principle behind the isoconversional methods is that the value of $f(\alpha)$ in Eq. 5 is independent of T. In other words, the value of $f(\alpha)$ is constant for a given α, irrespective of the temperature program. In its simplest form for non-isothermal conditions (the Friedman method), calculating isoconversional E_a involves plotting the values of $\ln(d\alpha/dt)$ against $1/T$ for a given α. The isoconversional approach enables changes in E_a to be detected during the reaction progress with no prior assumptions regarding the reaction mechanism. Such changes can, for example, reflect the changes in the bond strength with the reaction progress (Kuligiewicz & Derkowski, 2017).

Another calculation method based on the isoconversional principle and representing its simplified version is the method of Kissinger (1957). It is applicable to linear heating conditions and is based on the shift of the reaction peak when changing the heating rate, thus directly applicable to DTA, DSC, and DTG data (Fig. 10). This method employs the fact that for the maximum

reaction rate (DTG peak), $d^2\alpha/dt^2 = 0$. Taking this into account, the Kissinger equation can be derived from Eq. 7:

$$\ln\left(\frac{\beta}{T^2}\right) = \ln\left(-\frac{A\text{R}}{E_a}\frac{df(\alpha)}{d\alpha}\right) - \frac{E_a}{\text{R}}\frac{1}{T} \qquad (9)$$

where β is the linear heating rate (dT/dt). Values of all other parameters (T, $f(\alpha)$, and α) in Eq. 9 refer to values at the maximum reaction rate. In practice, the left side of Eq. 9 is plotted against $1/T$, which should produce a straight line, the slope of which can be used to calculate E_a (i.e.Vyazovkin, 2011; Fig. 11b).

Note that some studies apply kinetics analysis to data obtained from a single temperature program only (i.e. only one isothermal heating temperature or only one linear heating rate), which is especially common in the older literature. While this approach was justifiable because of hardware and computational limitations in those times, it is now generally considered unreliable (Vyazovkin et al., 2011).

Kinetics of Smectite Thermal Reactions

Dehydration

Despite the large number of studies of smectite–water interactions, kinetics studies of smectite dehydration employing thermal analysis methods do not present a consistent picture. Besides the dependence of dehydration energy on the hydration enthalpy of the interlayer cations (Webb et al., 1986), it has been demonstrated that a change occurs in the reaction mechanism along the course of dehydration (Koster van Groos & Guggenhem, 1990; Bray & Redfern, 1999; Kuligiewicz & Derkowski, 2017; Poinsignon et al., 1982; Zabat & Van Damme, 2000). As already mentioned, physisorbed water in the micro- and mesopores and bulk interlayer water represent the 'weakly-bound water' (WBW). WBW is removed preferentially during dehydration because of its weaker interactions with the smectite surface. Change in the reaction mechanism during dehydration and the associated change in E_a (Table 2) correspond to the completion of weakly bound water removal and the onset of strongly bound water removal. The E_a of dehydration of WBW is in the range 35–79 kJ/mol for smectites having monovalent and divalent interlayer cations commonly found in nature (Ca^{2+}, Mg^{2+},
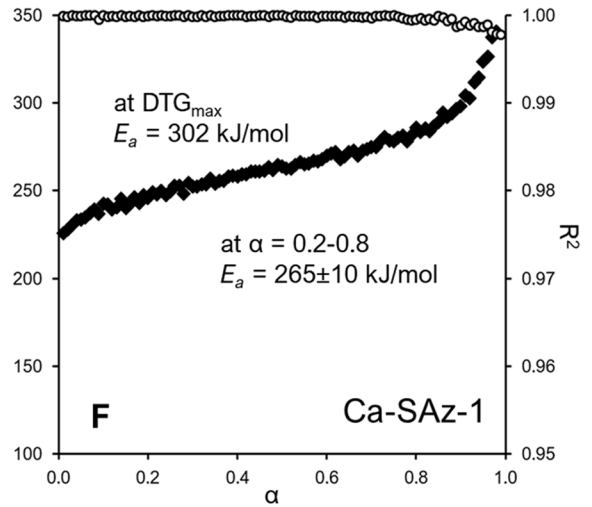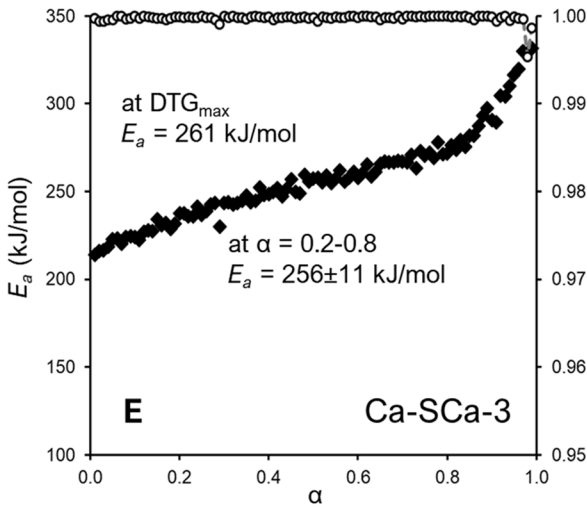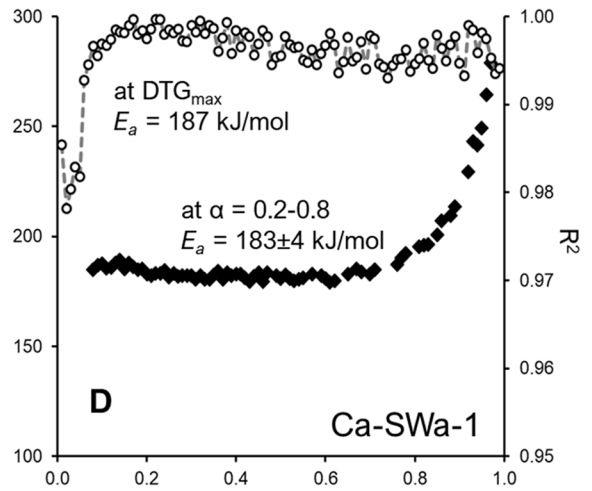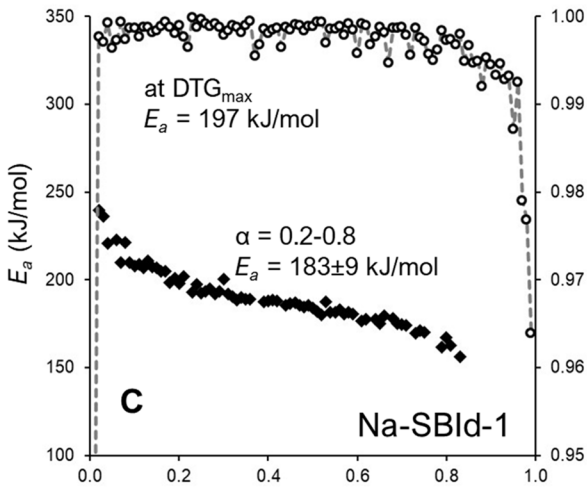
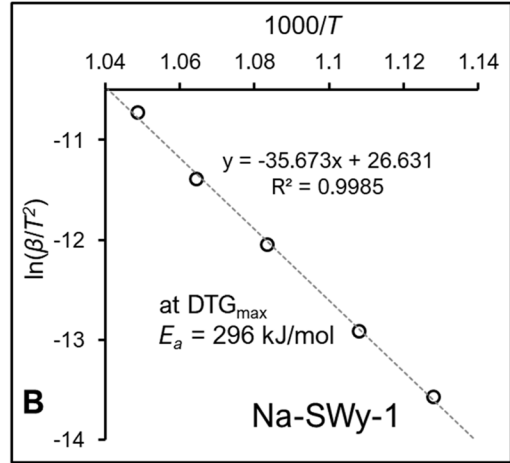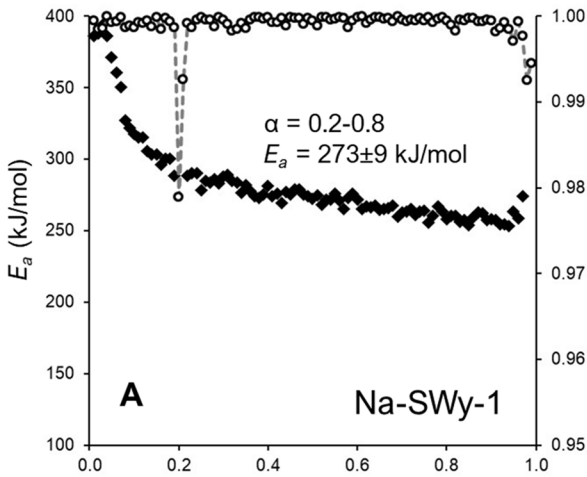◀**Fig. 11** **A**, C–F Activation energy (E_a) of the dehydroxylation of various dioctahedral smectites, calculated using the 0.01 α-increments and the Friedman method, and **B** an example of E_a determination using the Kissinger method and the DTG peak temperature (Fig. 10). Note the similarity of the E_a values and trends in the dehydroxylation of two Ca^{2+}-exchanged Mg-rich montmorillonites (**E**, **F**). For each TGA run, the total mass loss upon dehydroxylation was divided into 100 portions of equal mass difference (0.01α). For each 0.01α, the ln(dα/dt) was plotted against the corresponding 1/T using four or five data points from the TGA curves recorded with a different heating rate (**B**). **E** E_a is then calculated from the slope of ln(dα/dt) vs 1/T plot (Eq. 8). The correlation coefficient, R^2, was computed for each of 0.01α. All E_a values shown (**A**, **C–F**) are reported for $R^2 > 0.997$ (arbitrary cut-off),

K^+, Na^+, Li^+; Table 2). As deduced from Table 2, E_a of WBW dehydration in general does not depend on the exchangeable cation type or chemistry of the 2:1 layer. Once weakly bound water is removed, removal of the sequential portions of strongly bound water requires increasingly higher energy, as is manifested by the continuous increase in E_a with reaction progress, up to 190 kJ/mol (Kuligiewicz & Derkowski, 2017). This was interpreted as the result of bond reconfiguration upon removal of water molecules from hydration spheres of interlayer cations, in

Table 2 Comparison of the E_a of dehydration of weakly bound water (WBW) and strongly bound water (SBW) from studies employing various methods

Type of sample	E_a (kJ/mol)		Experimental method	Comments	Reference
	WBW	SBW			
Wyoming bentonite			Non-isothermal		Poinsignon et al. (1982)
Mg	35	121			
Ca	37	185			
Na	73				
K	79				
8 natural, predominantly Ca smectites	47–73		Non-isothermal, model fitting	No distinction between weakly- and strongly-bound water	Girgis et al. (1987)
Ca montmorillonite	35	~50	Isothermal, model fitting	Nucleation and growth mechanism was suggested for WBW and diffusion-controlled mechanism for SBW	Bray & Redfern (1999)
Wyoming montmorillonite			Non-isothermal, model-based*		Zabat & Van Damme (2000)
Na	42	–			
Cs	54	–			
Li	39	155			
Mg	38	46			
Ca	71	91			
Ba	43	111			
Al	87	89			
La	54	80			
SWy-1 Wyoming montmorillonite			DSC Kissinger method, using various $P–T$ conditions and H_2O activity		Koster van Groos & Guggenheim (1987, 1990)
K	46	56			
Ca	49	58			
Mg	49	66			
Mg-SCa-3	–	88–161	Non-isothermal, isoconversional	E_a of WBW or SBW for some samples could not be calculated due to differences in experiment design	Kuligiewicz and Derkowski (2017)
Ca-SCa-3	48	102–189			
Na-SCa-3	49	87–185			
Mg-SAz-2	–	76–139			
Ca-SAz-2	52	–			
Na-SAz-2	53	–			
Ca-SWy-2	45	–			
Na-SWy-2	47	–			

*Zabat and Van Damme (2000) assumed the first-order reaction mechanism for dehydration and presented a new computation method, using principles similar to those of the Kissinger method

agreement with theoretical calculations (Pavlov et al., 1998).

Dehydroxylation

In the majority of dioctahedral smectites studied, E_a of dehydroxylation does not vary much with the reaction progress (Fig. 11A,C,D). If the initial ($\alpha < 0.2$) and final ($\alpha > 0.8$) portions of the data, corresponding also to lower R^2 coefficients because of an overlap with other thermal effects are excluded, the E_a values remain similar over a broad range of α for beidellite SBId-1, *cv* beidellitic montmorillonite SWy-1, and ferruginous smectite SWa-1 (an approximation for nontronite) (Fig. 11). In Mg-rich montmorillonites that have charge generated exclusively in the octahedral sheet, however, E_a increases significantly with α, especially in the samples saturated with divalent cations (Fig. 11E,F). The increase of E_a in montmorillonite remains in line with the interpretation of Koster van Groos and Guggenheim (1989) who suggested the increase in the residual OH bond strength upon sequential removal of OH groups in heterogeneous structure.

The kinetics of smectite dehydroxylation is controlled by the same structural factors as the temperature of dehydroxylation (Figs. 1 and 3). Activation energy of dehydroxylation as computed from linear heating experiments with isoconversional methods correlates linearly with the temperature of maximum dehydroxylation, based on the DTG peak (Fig. 12, Table 3). The observed relationship implies that the rate-controlling mechanism of dehydroxylation is the same in all smectites regardless of their crystal-chemical composition.

Another factor influencing the kinetics of smectite dehydroxylation is the interlayer cation type. The application of the model-fitting approach to isothermal data allowed demonstration that the interlayer cation type can modify the dominant reaction model, which provides the best description of the process. Bray and Redfern (2000) suggested that dehydroxylation in smectite saturated with divalent cations (Ca^{2+} or Mg^{2+}) is diffusion-controlled, while dehydroxylation in smectites saturated with monovalent cations (Na^+ or K^+) follows the first-order reaction kinetics. The influence of the interlayer cation on the dehydroxylation E_a value is less clear (Bray & Redfern, 2000; Kuligiewicz & Derkowski, 2017) but it
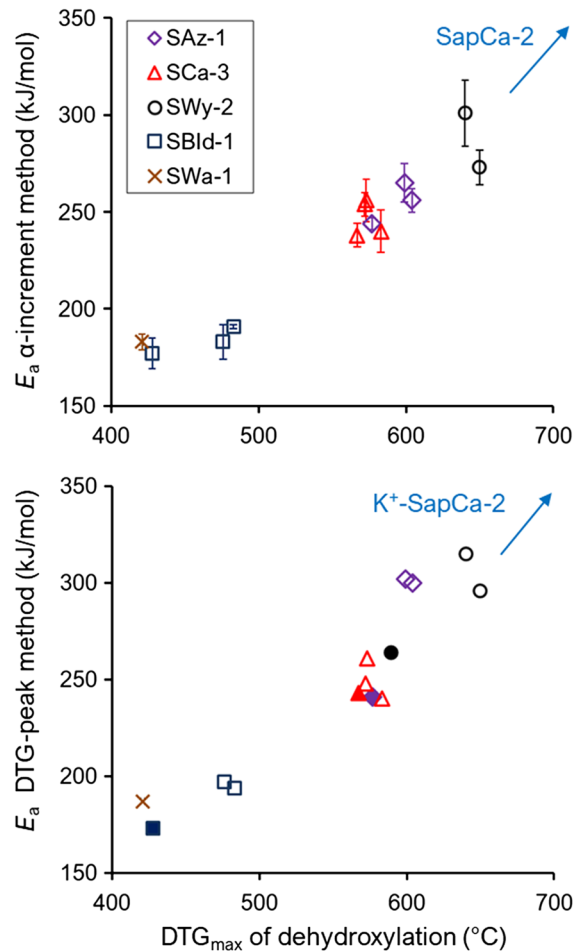

Fig. 12 The E_a of dehydroxylation of smectite reference samples presenting values averaged over $\alpha = 0.2$–0.8 calculated using the Friedman method (upper, cf. Figure 11) and E_a calculated using the conventional Kissinger method based on DTG peak temperature (lower, cf. Fig. 10), plotted against the maximum of dehydroxylation (DTG$_{max}$; Table 3). The E_a error in the Kissinger method is ~5%. Filled shapes denote the Cs^+-exchanged form; note their lower position with respect to other cations

seems that Mg^{2+}-exchanged smectites have significantly lower E_a values than Ca^{2+}- or Na^+-exchanged counterparts (Bray & Redfern, 2000; Kuligiewicz & Derkowski, 2017). A speculative explanation may be that Mg^{2+}, which is capable of retaining dissociated H_2O (Mg-OH) up to temperatures of dehydroxylation, acts as a flux and lowers the E_a of dehydroxylation.

All of the above-mentioned results and interpretations come from studies using simple (isothermal or linear heating rate) thermal experiments. An alternative approach based on multiple heating–cooling cycles was employed by Drits et al. (2012a) to

Table 3 E_a of dehydroxylation calculated as using the 0.01 α-increments with values averaged over α = 0.2–0.6 calculated using the Friedman method (Fig. 11) and E_a calculated using the conventional Kissinger method based on DTG peak temperature (Fig. 10). The maximum of dehydroxylation (DTG_{max}) was determined using the 5°C/min constant rate TG measurement

Smectite sample and interlayer cation	Octahedral vacancy	DTG_{max} (°C)	Average $E_a \pm SD$ (kJ/mol) see Figure 11	E_a (kJ/mole) Kissinger method*
Ca-SAz-1	*tv*	599	265 ± 10	302
Na-SAz-1	*tv*	604	256 ± 6	300
Ca-SAz-1	*tv*	577	244 ± 3	241
Ca-SCa-3	*tv*	573	256 ± 11	261
Na-SCa-3	*tv*	572	254 ± 6	248
Mg-SCa-3	*tv*	583	240 ± 11	240
Cs-SCa-3	*tv*	567	238 ± 6	243
Ca-SWy-1	*cv*	640	301 ± 17	315
Na-SWy-1	*cv*	650	273 ± 9	296
Cs-SWy-1	*cv*	589	–	264
Ca-SBId-1	*tv*	483	191 ± 1	194
Na-SBId-1	*tv*	476	183 ± 9	197
Cs-SBId-1	*tv*	428	177 ± 8	173
Ca-SWa-1	*tv*	421	183 ± 4	187
K-SapCa-2	trioct	852	521 ± 25	574

*estimated E_a error in the Kissinger method is ~5% relative

determine the kinetics of partial dehydroxylation in dioctahedral smectites and other 2:1 layer minerals. The protocol involves heating the samples with a constant heating rate and subsequent cooling by increasing each following cycle's maximum temperature in small increments (i.e. 25°C). If a temperature increment between cycles is sufficiently small, the increase of α within one and the same cycle is negligible; therefore, α can be considered as constant for the cycle, meeting the requirement of the isoconversional kinetic approach. Within the cycle, the majority of the ln(dα/d*t*) over 1/*T* returns a linear fit, which Drits et al. (2012a) interpreted as the zeroth-order kinetics of partial dehydroxylation. Such a heating–cooling cycle approach apparently allows tracking of E_a in different stages of the reaction or portions of sample reacted at subsequently higher temperatures. However, for a portion of the sample reacting with constant $f(α)$, the Arrhenius relationship represents the population that has already been treated thermally in the preceding cycle, hence, not corresponding to the actual rate-controlling mechanism in full reaction (Muñoz-Santiburcio et al., 2012; Ogloza & Malhotra, 1989). The difficulty in explaining the concave shape of E_a evolution over α (Fig. 13) and the maximum E_a being much lower than that for full reaction (Figs. 11 and 12) implies the limited use of the heating–cooling protocol and the need for specific interpretation of the kinetic data.

Rehydration and Rehydroxylation

The kinetics of smectite rehydration is methodologically challenging to study because the maximum amount of water which can be adsorbed by the smectite's structure is dependent on temperature; for a fixed H_2O molar content in the carrier gas, the lower the reaction temperature, the greater the rehydration (Fig. 6), but for constant RH the degree of rehydration is likely to be similar in spite of different temperatures (Vieillard et al., 2019). This renders non-isothermal experiments inapplicable. The rehydration process can be most conveniently tracked using the TGA experimental setup, allowing in situ dehydration and rehydration (Derkowski & Kuligiewicz, 2017). The mechanism of rehydration at temperatures <100°C cannot be described well by a commonly used solid-state reaction model (such as those presented in Table 1 of Khawam & Flanagan, 2006a). Models developed specifically for adsorption kinetics,
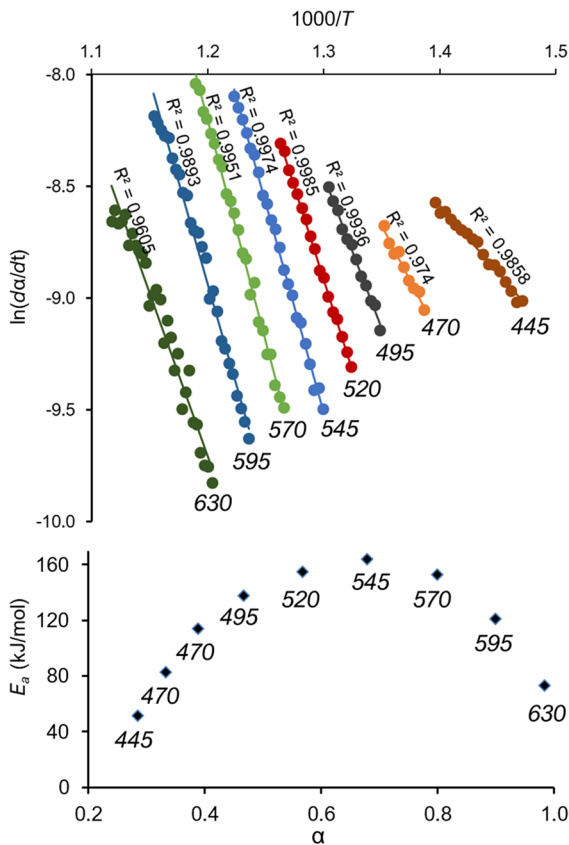
Fig. 13 An example of the calculation of E_a of smectite dehydroxylation for Ca^{2+}-saturated SCa-3 montmorillonite based on a heating–cooling cycles TGA experiment (Drits et al., 2012a). The maximum temperature (in °C) of each consecutive heating cycle is given in italics. Compare E_a values with Fig. 11e

such as a pseudo n^{th} order model, usually provide much better description of the process (see Largitte & Pasquier, 2016, for a comprehensive review of models used in the adsorption kinetics). Rehydration kinetics are influenced by the exchangeable cation type; cations with low hydration energy (such as Cs^+) adsorb quickly the small amount of water which they are capable of holding. For smectite saturated with cations with high hydration energy (such as Mg^{2+}), the adsorption process continues over longer timescales (Fig. 6).

Isothermal rehydroxylation experiments under H_2O vapor at temperatures above those typical for rehydration have shown that kinetics of smectite rehydroxylation can be described by the time-to-the-quarter (TTTQ) model expressed as relative mass gain equal to the temperature-dependent rate constant

multiplied by the 4th root of reaction time (Hamilton & Hall, 2012; Derkowski & Kuligiewicz, 2017). Explained as corresponding to restricted, single-file diffusion in fired clay minerals, the TTTQ model has been applied to clay-based traditional ceramics and used to predict the time elapsed since firing, hence for archeological dating (Hare et al., 2016; Wilson et al., 2009). Both the root coefficient of the TTTQ (Barret, 2017) and the overall validity of TTTQ model for kinetic calculations have been criticized strongly (Kuligiewicz & Derkowski, 2021).

Studies of E_a of smectite rehydroxylation are still rare and the E_a values calculated based on the TTTQ model remain within an unexpectedly broad range, between 19 and 173 kJ/mol for experiments performed at 110–400°C (Derkowski & Kuligiewicz, 2017; Stevenson & Gurnick, 2016). However, Kuligiewicz and Derkowski (2021) recently proved that the TTTQ model describes well the progress of various reactions governed by unexpectedly different mechanisms. E_a obtained with the TTTQ model for those reactions was grossly incorrect despite an apparent agreement with simulated data, making the TTTQ model unreliable. Therefore, although the TTTQ model fits well the smectite isothermal rehydroxylation in some cases and has served for occasional successful dating of clay ceramics, its link to kinetics formalism and the mechanism of rehydroxylation are still unclear and a need exists to develop an alternative approach.

Declarations

References

Barrett, G. T. (2017). Rehydroxylation (RHX) dating: Trials on post-medieval brick using a component based approach. *Journal of Archaeological Science: Reports, 16*, 489–502.

Berend, I., Cases, J. M., Francois, M., Uriot, J. P., Michot, L., Masion, A., & Thomas, F. (1995). Mechanism of adsorption and desorption of water vapor by homoionic montmorillonites; 2, The Li^+, Na^+, K^+, Rb^+ and Cs^+-exchanged forms. *Clays and Clay Minerals, 43*(3), 324–336.

Bish, D. L. & Duffy, C. J. (1990). Thermogravimetric Analysis of Minerals. In Stucki, J.W., Bish, D., & Mumpton, F. A. (Eds), *CMS Workshop Lectures, vol. 3. Thermal analysis in clay science*. The Clay Minerals Society. https://doi.org/10.1346/CMS-WLS-3.4

Boller, A., Jin, Y., & Wunderlich, B. (1994). Heat capacity measurement by modulated DSC at constant temperature. *Journal of Thermal Analysis and Calorimetry, 42*(2–3), 307–330.

Botella, V., Timón, V., Escamilla-Roa, E., Hernandez-Languna, A., & Sainz-Díaz, C. I. (2004). Hydrogen bonding and vibrational properties of hydroxy groups in the crystal lattice of dioctahedral clay minerals by means of first principles calculations. *Physics and Chemistry of Minerals, 31*(8), 475–486.

Bottom, R. (2008). Thermogravimetric Analysis. In P. Gabbott (Ed.), *Principles and applications of thermal analysis*. John Wiley & Sons.

Bradley, W. F., & Grim, R. E. (1951). High temperature thermal effects of clay and related materials. *American Mineralogist, 36*(3–4), 182–201.

Bray, H. J., & Redfern, S. A. T. (1999). Kinetics of dehydration of Ca-montmorillonite. *Physics and Chemistry of Minerals, 26*(7), 591–600.

Bray, H. J., & Redfern, S. A. T. (2000). Influence of counterion species on the dehydroxylation of Ca^{2+}-, Mg^{2+}-, Na^+-and K^+-exchanged Wyoming montmorillonite. *Mineralogical Magazine, 64*(2), 337–346.

Brett, N. H., MacKenzie, K. J. D., & Sharp, J. H. (1970). The thermal decomposition of hydrous layer silicates and their related hydroxides. *Quarterly Reviews, Chemical Society, 24*(2), 185–207.

Byrn, S. R., Zografi, G., & Chen, X. S. (2017). Differential scanning calorimetry and thermogravimetric analysis. *Solid State Properties of Pharmaceutical Materials* (pp. 124–142). Wiley.

Cases, J. M., Bérend, I., François, M., Uriot, L. P., Michot, L. J., & Thomas, F. (1997). Mechanism of adsorption and desorption of water vapor by homoionic montmorillonite: 3. The Mg^{2+}, Ca^{2+}, Sr^{2+} and Ba^{2+} exchanged forms. *Clays and Clay Minerals, 45*(1), 8–22.

Christidis, G. E., Aldana, C., Chryssikos, G. D., Gionis, V., Kalo, H., Stöter, M., Breu, J., & Robert, J. L. (2018). The nature of laponite: pure hectorite or a mixture of different trioctahedral phases? *Minerals, 8*(8), 314.

Criado, J., Sánchez-Jiménez, P., & Pérez-Maqueda, L. (2008). Critical study of the isoconversional methods of kinetic analysis. *Journal of Thermal Analysis and Calorimetry, 92*(1), 199–203.

Cuadros, J. (2002). Structural insights from the study of Cs-exchanged smectites submitted to wetting-and-drying cycles. *Clay Minerals, 37*(3), 473–486.

Dainyak, L. G., Dritz, V. A., Kudryavtzev, D. I., Simanovitch, I. M., & Slonimskaya, M. V. (1981). Novaya mineral'naya raznovidnost' trioktaedricheskech smektitov iz effuzivnych basaltov Tungusskoi sineklizy (New mineral variant of trioctahedral smectites from effusive basalts of Tungusskaya sineclise). *Lithology and Mineral Resources, 6*, 123129. (in Russian).

Della Gatta, G., Richardson, M. J., Sarge, S. M., & Stølen, S. (2006). Standards, calibration, and guidelines in microcalorimetry. Part 2. Calibration standards for differential scanning calorimetry (IUPAC Technical Report). *Pure and Applied Chemistry, 78*(7), 1455–1476.

Derkowski, A., & Kuligiewicz, A. (2017). Rehydroxylation in smectites and other clay minerals observed in-situ with a modified thermogravimetric system. *Applied Clay Science, 136*, 219–229.

Derkowski, A., Drits, V. A., & McCarty, D. K. (2012). Nature of rehydroxylation in dioctahedral 2:1 layer clay minerals. *American Mineralogist, 97*, 610–629.

Derkowski, A., Drits, V. A., & McCarty, D. K. (2012). Rehydration in a dehydrated-dehydroxylated smectite in environment of low water vapor content. *American Mineralogist, 97*, 110–127.

Dietel, J., Warr, L. N., Bertmer, M., Steudel, A., Grathoff, G. H., & Emmerich, K. (2017). The importance of specific surface area in the geopolymerization of heated illitic clay. *Applied Clay Science, 139*, 99–107.

Ding, Z., & Frost, R. L. (2002). Controlled rate thermal analysis of nontronite. *Thermochimica Acta, 389*(1–2), 185–193.

Drits, V. A., & Zviagina, B. (2009). Trans-vacant and cis-vacant 2:1 layer silicates: Structural features, identification, and occurrence. *Clays and Clay Minerals, 57*(4), 405–415.

Drits, V. A., Besson, G., & Muller, F. (1995). An improved model for structural transformation of heat-treated aluminous dioctahedral 2:1 layer silicates. *Clays and Clay minerals, 43*(6), 718–731.

Drits, V. A., Lindgreen, H., Salyn, A. L., Ylagan, R., & McCarty, D. K. (1998). Semiquantitative determination of trans-vacant and cis-vacant 2: 1 layers in illites and illite-smectites by thermal analysis and X-ray diffraction. *American Mineralogist, 83*(12), 1188–1198.

Drits, V. A., Derkowski, A., & McCarty, D. K. (2012). Kinetics of partial dehydroxylation in dioctahedral 2:1 layer clay minerals. *American Mineralogist, 97*, 930–950.

Drits, V. A., McCarty, D. K., & Derkowski, A. (2012). Mixed-layered structure formation during trans-vacant Al-rich illite dehydroxylation. *American Mineralogist, 97*, 1922–1938.

El-Barawy, K. A., Girgis, B. S., & Felix, N. S. (1986). Thermal treatment of some pure smectites. *Thermochimica Acta, 98*, 181–189.

Emmerich, K. (2000). Spontaneous rehydroxylation of a dehydroxylated cis-vacant montmorillonite. *Clays and Clay Minerals, 48*(3), 405–408.

Emmerich, K. (2010). Thermal Analysis in the Characterization and Processing of Industrial Minerals. In G. E. Christidis (Ed.), *Advances in the Characterization of Industrial Minerals.* European Mineralogical Union.

Emmerich, K., & Smykatz-Kloss, W. (2002). Exothermic effects in soils during thermal analysis. *Clay Minerals, 37*(4), 575–582.

Emmerich, K., Madsen, F. T., & Kahr, G. (1999). Dehydroxylation behavior of heat-treated and steam-treated homoionic cis-vacant montmorillonites. *Clays and Clay Minerals, 47*(5), 591–604.

Emmerich, K., Plötze, M., & Kahr, G. (2001). Reversible collapse and Mg^{2+} release of de-and rehydroxylated homoionic cis-vacant montmorillonites. *Applied Clay Science, 19*(1–6), 143–154.

Emmerich, K., Wolters, F., Kahr, G., & Lagaly, G. (2009). Clay profiling: the classification of montmorillonites. *Clays and Clay Minerals, 57*(1), 104–114.

Emmerich, K., Steudel, A., & Merz, D. (2017). Dehydroxylation of dioctahedral smectites in water vapor atmosphere. *Applied Clay Science, 137*, 1–5.

Emmerich, K., Giaudo, N., Schuhmann, R., Schnetzer, F., Kaden, H., & Thissen, P. (2018). On the Prediction of Water Contents in Na-Saturated Dioctahedral Smectites. *Journal of Physical Chemistry C, 122*(13), 7484–7493.

Farmer, V. C., Russell, J. D., McHardy, W. J., Newman, A. C. D., Ahlrichs, J. L., & Rimsaite, J. Y. H. (1971). Evidence for loss of protons and octahedral iron from oxidized biotites and vermiculites. *Mineralogical Magazine, 38*(294), 121–137.

Ferrage, E., Lanson, B., Michot, J. L., & Robert, J.-L. (2010). Hydration properties and interlayer organization of water and ions in synthetic Na-smectite with tetrahedral layer charge. Part 1. Results from X-ray diffraction profile modeling. *Journal of Physical Chemistry C, 114*, 4515–4526.

Gabbott, P. (2008). *Principles and applications of thermal analysis.* John Wiley & Sons.

Gailhanou, H., Vieillard, P., Blanc, P., Lassin, A., Denoyel, R., Bloch, E., De Weireld, G., Gaboreau, S., Fialips, C. I., Madé, B., & Giffaut, E. (2017). Methodology for determining the thermodynamic properties of smectite hydration. *Applied Geochemistry, 82*, 146–163.

Garg, N., & Skibsted, J. (2014). Thermal activation of a pure montmorillonite clay and its reactivity in cementitious systems. *The Journal of Physical Chemistry C, 118*(21), 11464–11477.

Giese, R. F. (1990). Precision Scanning Calorimetry of Clay Minerals and Their Intercalates: In Stucki, J. W., Bish, D., & Mumpton F. A. (Eds), *CMS Workshop Lectures, Vol. 3. Thermal analysis in clay science.* The Clay Minerals Society. https://doi.org/10.1346/CMS-WLS-3.2

Girgis, B. S., El-Barawy, K. A., & Felix, N. S. (1987). Dehydration kinetics of some smectites: a thermogravimetric study. *Thermochimica Acta, 111*, 9–19.

Grekov, D., Montavon, G., Robinet, J. C., & Grambow, B. (2019). Smectite fraction assessment in complex natural clay rocks from interlayer water content determined by thermogravimetric and thermoporometry analysis. *Journal of Colloid and Interface Science, 555*, 157–165.

Grim, R. E., & Bradley, W. F. (1940). Investigation of the effect of heat on the clay minerals illite and montmorillonite. *Journal of the American Ceramic Society, 23*(8), 242–248.

Grim, R. E., & Rowland, R. A. (1942). Differential thermal analyses of clay minerals and other hydrous materials. Part 1. *American Mineralogist, 27*, 746–761.

Grim, R. E., & Rowland, R. A. (1942). Differential thermal analyses of clay minerals and other hydrous materials. Part 2. *American Mineralogist, 27*, 901–818.

Guggenheim, S. (1990). The dynamics of thermal decomposition in aluminous dioctahedral 2: 1 layer silicates: A crystal chemical model. *Sciences Géologiques, Bulletins et Mémoires, 86*(1), 99–107.

Guggenheim, S., Chang, Y. H., & Koster van Groos, A. F. (1987). Muscovite dehydroxylation; high-temperature studies. *American Mineralogist, 72*(5–6), 537–550.

Hamilton, A., & Hall, C. (2012). A review of rehydroxylation in fired-clay ceramics. *Journal of the American Ceramic Society, 95*(9), 2673–2678.

Hare, V. J., Kärger, J., Moinester, M., & Piasetzky, E. (2016). Testing the (time)$^{1/4}$ diffusion law of rehydroxylation in fired clays: evidence for single-file diffusion in porous media? *Diffusion fundamentals Organization, 25*(5), 1–11.

Heide, K., & Földvari, M. (2006). High temperature mass spectrometric gas-release studies of kaolinite $Al_2[Si_2O_5(OH)_4]$ decomposition. *Thermochimica Acta, 446*(1–2), 106–112.

Heller-Kallai, L. (1997). Reduction and reoxidation of nontronite: the data reassessed. *Clays and Clay Minerals, 45*(3), 476–479.

Heller-Kallai, L. (1997). The nature of clay volatiles and condensates and the effect on their environment: A review. *Journal of Thermal Analysis and Calorimetry, 50*(1–2), 145–156.

Heller-Kallai, L., & Rozenson, L. (1980). Dehydroxylation of dioctahedral phyllosilicates. *Clays and Clay Minerals, 28*(5), 355–368.

Hofmann, U., & Klemen, R. (1950). Verlust der austauschfähigkeit von lithiumionen an bentonit durch erhitzung. *Zeitschrift für Anorganische Chemie, 262*(1–5), 95–99.

Hofmann, U., Endell, K., & Wilm, D. (1933). Kristallstruktur und quellung von montmorillonit. *Zeitschrift für Kristallographie-Crystalline Materials, 86*(1–6), 340–348.

Jackson, M. L. (1969). *Soil Chemical Analysis: Advanced Course.* Edition 2 pp. 895 pp. UW-Madison.

Kanik, N. J., Longstaffe, F. J., Kuligiewicz, A., & Derkowski, A. (2022). Systematics of smectite hydrogen-isotope composition: structural hydrogen versus adsorbed water. *Applied Clay Science, 216*, 106338.

Kawano, M., & Tomita, K. (1989). X-ray studies of rehydration behaviors for montmorillonite. *Clay Science, 7*(5), 277–287.

Kawano, M., & Tomita, K. (1991). Dehydration and rehydration of saponite and vermiculite. *Clays and Clay Minerals, 39*(2), 174–183.

Kawano, M., & Tomita, K. (1991). X-ray powder diffraction studies on the rehydration properties of beidellite. *Clays and Clay Minerals, 39*(1), 77–83.

Khawam, A., & Flanagan, D. R. (2006). Basics and Applications of Solid-State Kinetics: A Pharmaceutical Perspective. *Journal of Pharmaceutical Sciences, 95*(3), 472–498.

Khawam, A., & Flanagan, D. R. (2006). Solid-State Kinetic Models: Basics and Mathematical Fundamentals. *The Journal of Physical Chemistry B, 110*(35), 17315–17328.

Kissinger, H. E. (1957). Reaction kinetics in differential thermal analysis. *Analytical Chemistry, 29*, 1702–1706.

Kohyama, N., Shimoda, S., & Sudo, T. (1973). Iron-rich saponite (ferrous and ferric forms). *Clays and Clay Minerals, 21*(4), 229–237.

Komadel, P., Hrobáriková, J., & Koppelhuber-Bitschnau, B. (2002). Hydration of reduced-charge montmorillonite. *Clay Minerals, 37*(3), 543–550.

Komadel, P., Madejová, J., & Bujdák, J. (2005). Preparation and properties of reduced-charge smectites–a review. *Clays and Clay Minerals, 53*(4), 313–334.

Koster van Groos, A. F. & Guggenheim, S. (1990). High pressure Differential Thermal Analysis of Clays. In Stucki, J. W., Bish, D., & Mumpton F. A. (Eds.), *CMS Workshop Lectures, Vol. 3. Thermal Analysis in Clay Science*. The Clay Minerals Society. https://doi.org/10.1346/CMS-WLS-3.3

Koster van Groos, A. F., & Guggenheim, S. (1987). Dehydration of a Ca-and a Mg-exchanged montmorillonite (SWy-1) at elevated pressures. *American Mineralogist, 72*(3–4), 292–298.

Koster van Groos, A. F., & Guggenheim, S. (1989). Dehydroxylation of Ca-and Mg-exchanged montmorillonite. *American Mineralogist, 74*(5–6), 627–636.

Kuligiewicz, A., & Derkowski, A. (2017). Tightly bound water in smectites. *American Mineralogist, 102*, 1073–1090.

Kuligiewicz, A., & Derkowski, A. (2021). Rehydroxylation of fired clays: is the time to the quarter (TTTQ) model correct? *Journal of Archaeological Science, 125*, 105301.

Kuligiewicz, A., Derkowski, A., Szczerba, M., Gionis, V., & Chryssikos, G. D. (2015). Revisiting the infrared spectrum of the water–smectite interface. *Clays and Clay Minerals, 63*, 15–29.

Largitte, L., & Pasquier, R. (2016). A review of the kinetics adsorption models and their application to the adsorption of lead by an activated carbon. *Chemical Engineering Research and Design, 109*, 495–504.

Le Chatelier, M. H. (1887). De l'action de la chaleur sur les argiles. *Bulletin de la Société française de Minéralogie, 10*(5–6), 204–211.

Lear, P. R., & Stucki, J. W. (1985). Role of structural hydrogen in the reduction and reoxidation of iron in nontronite. *Clays and Clay Minerals, 33*(6), 539–545.

Lempart, M., Derkowski, A., Luberda-Durnaś, K., Skiba, M., & Błachowski, A. (2018). Dehydrogenation and dehydroxylation as drivers of the thermal decomposition of Fe-chlorites. *American Mineralogist, 103*(11), 1837–1850.

Lempart, M., Derkowski, A., Strączek, T., & Kapusta, C. (2020). Systematics of H_2 and H_2O evolved from chlorites during oxidative dehydrogenation. *American Mineralogist, 105*, 932–944.

Levy, J. H., & Hurst, H. J. (1993). Kinetics of dehydroxylation, in nitrogen and water vapour, of kaolinite and smectite from Australian Tertiary oil shales. *Fuel, 72*(6), 873–877.

Levy, J. H., & White, T. J. (1988). The reaction of pyrite with water vapour. *Fuel, 67*(10), 1336–1339.

MacKenzie, K. J. D., & Berezowski, R. M. (1984). Thermal and Mössbauer studies of iron-containing hydrous silicates. V. Berthierine. *Thermochimica Acta, 74*(1–3), 291–312.

MacKenzie, K. J. D., & Rogers, D. E. (1977). Thermal and Mössbauer studies of iron-containing hydrous silicates: I. nontronite. *Thermochimica Acta, 18*(2), 177–196.

Mackenzie, R. C., & Bishui, B. M. (1958). The montmorillonite differential thermal curve. II. Effect of exchangeable cations on the dehydroxylation of normal montmorillonite. *Clay Minerals Bulletin, 3*(20), 276–286.

Meija, J., Mester, Z., & D'Ulivo, A. (2006). Mass spectrometric separation and quantitation of overlapping isotopologues $H_2O/HOD/D_2O$ and $H_2Se/HDSe/D_2Se$ mixtures. *Journal of the American Society for Mass Spectrometry, 17*(7), 1028–1036.

Meyers, K. S., & Speyer, R. F. (2003). Thermal analysis of clays. *In Handbook of Thermal Analysis and Calorimetry* (2nd ed.). Elsevier Science BV, pp. 261–306

Mikutta, R., Kleber, M., Kaiser, K., & Jahn, R. (2005). Organic matter removal from soils using hydrogen peroxide, sodium hypochlorite, and disodium peroxodisulfate. *Soil Science Society of America Journal, 69*(1), 120–135.

Molina-Montes, E., Timón, V., Hernández-Laguna, A., & Sainz-Díaz, C. I. (2008). Dehydroxylation mechanisms in Al^{3+}/Fe^{3+} dioctahedral phyllosilicates by quantum mechanical methods with cluster models. *Geochimica et Cosmochimica Acta, 72*(16), 3929–3938.

Muller, F., Drits, V. A., Plançon, A., & Besson, G. (2000). Dehydroxylation of Fe3+, Mg-rich dioctahedral micas:(I) structural transformation. *Clay Minerals, 35*(3), 491–504.

Muller, F., Drits, V. A., Plançon, A., & Robert, J. P. (2000). Structural transformation of 2:1 dioctahedral layer silicates during dehydroxylation-rehydroxylation reactions. *Clays and Clay Minerals, 48*, 572–585.

Muñoz-Santiburcio, D., Kosa, M., Hernández-Laguna, A., Sainz-Díaz, C. I., & Parrinello, M. (2012). Ab initio molecular dynamics study of the dehydroxylation reaction in a smectite model. *The Journal of Physical Chemistry C, 116*(22), 12203–12211.

Ngouana, B. F., & Kalinichev, A. G. (2014). Structural arrangements of isomorphic substitutions in smectites: Molecular simulation of the swelling properties, interlayer structure, and dynamics of hydrated Cs-montmorillonite revisited with new clay models. *The Journal of Physical Chemistry C, 118*(24), 12758–12773.

Ogloza, A. A., & Malhotra, V. M. (1989). Dehydroxylation induced structural transformations in montmorillonite: an isothermal FTIR study. *Physics and Chemistry of Minerals, 16*(4), 378–385.

Pavlov, M., Siegbahn, P. E., & Sandström, M. (1998). Hydration of beryllium, magnesium, calcium, and zinc ions using density functional theory. *The Journal of Physical Chemistry A, 102*(1), 219–228.

Pelletier, M., Michot, L. J., Humbert, B., Barrès, O., de la Caillerie, J. B. D., & Robert, J.-L. (2003). Influence of layer charge on the hydroxyl stretching of trioctahedral clay minerals: A vibrational study of synthetic Na- and K-saponites. *American Mineralogist, 88*, 1801–1808.

Pérez-Maqueda, L. A., Blanes, J. M., Pascual, J., & Pérez-Rodríguez, J. L. (2004). The influence of sonication on the thermal behavior of muscovite and biotite. *Journal of the European Ceramic Society, 24*(9), 2793–2801.

Perez-Rodriguez, J. L., Duran, A., Sanchez Jimenez, P. E., Franquelo, M. L., Perejón, A., Pascual-Cosp, J., & Pérez-Maqueda, L. A. (2010). Study of the dehydroxylation–rehydroxylation of pyrophyllite. *Journal of the American Ceramic Society, 93*(8), 2392–2398.

Plante, A. F., Fernández, J. M., & Leifeld, J. (2009). Application of thermal analysis techniques in soil science. *Geoderma, 153*(1–2), 1–10.

Poinsignon, C., Yvon, J., & Mercier, R. (1982). Dehydration energy of the exchangeable cations in montmorillonite—A DTA study. *Israel Journal of Chemistry, 22*(3), 253–255.

Rancourt, D. G., Mercier, P. H. J., Cherniak, D. J., Desgreniers, S., Kodama, H., Robert, J. L., & Murad, E. (2001). Mechanisms and crystal chemistry of oxidation in annite: resolving the hydrogen-loss and vacancy reactions. *Clays and Clay Minerals, 49*(6), 455–491.

Rouquerol, F., Rouquerol, J., & Llewellyn, P. (2013). *Thermal analysis*. In: Developments in Clay Science (Vol. 5, pp. 361–379). Elsevier.

Salles, F., Douillard, J. M., Denoyel, R., Bildstein, O., Jullien, M., Beurroies, I., & Van Damme, H. (2009). Hydration sequence of swelling clays: Evolutions of specific surface area and hydration energy. *Journal of Colloid and Interface Science, 333*(2), 510–522.

Salles, F., Bildstein, O., Douillard, J. M., Jullien, M., Raynal, J., & Van Damme, H. (2010). On the cation dependence of interlamellar and interparticular water and swelling in smectite clays. *Langmuir, 26*(7), 5028–5037.

Salles, F., Douillard, J. M., Bildstein, O., El Ghazi, S., Prélot, B., Zajac, J., & Van Damme, H. (2015). Diffusion of interlayer cations in swelling clays as a function of water content: Case of montmorillonites saturated with alkali cations. *The Journal of Physical Chemistry C, 119*(19), 10370–10378.

Sanz, J., Gonzalez-Carreno, T., & Gancedo, R. (1983). On dehydroxylation mechanisms of a biotite in vacuo and in oxygen. *Physics and Chemistry of Minerals, 9*(1), 14–18.

Schilling, M. R. (1990). Effects of sample size and packing in the thermogravimetric analysis of calcium montmorillonite STx-1. *Clays and Clay Minerals, 38*(5), 556–558.

Seiffarth, T., & Kaps, C. (2009). Structural characterization of (Cu^{2+}, Na^+)- and (Cu^{2+}, NH_4^+)-exchanged bentonites upon thermal treatment. *Clays and Clay Minerals, 57*(1), 40–45.

Shannon, R. D. (1976). Revised effective ionic radii and systematic studies of interatomic distances in halides and chalcogenides. *Acta Crystallographica A, 32*(5), 751–767.

Sidey, V. (2016). On the effective ionic radii of ammonium. *Acta Crystallographica B., B72*, 626–633.

Skoubris, E. N., Chryssikos, G. D., Christidis, G. E., & Gionis, V. (2013). Structural characterization of reduced-charge montmorillonites. Evidence based on FTIR spectroscopy, thermal behavior, and layer-charge systematics. *Clays and Clay Minerals, 61*(2), 83–97.

Smith, D. W. (1977). Ionic hydration enthalpies. *Journal of Chemical Education, 54*(9), 540.

Środoń, J. (2009). Quantification of illite and smectite and their layer charges in sandstones and shales from shallow burial depth. *Clay Minerals, 44*(4), 421–434.

Środoń, J., & McCarty, D. K. (2008). Surface area and layer charge of smectite from CEC and $EGME/H_2O$-retention measurements. *Clays and Clay Minerals, 56*(2), 155–174.

Środoń, J., Zeelmaekers, E., & Derkowski, A. (2009). The charge of component layers of illite-smectite in bentonites and the nature of end-member illite. *Clays and Clay Minerals, 57*(5), 649–671.

Stackhouse, S., Coveney, P. V., & Benoit, D. M. (2004). Density-functional-theory-based study of the dehydroxylation behavior of aluminous dioctahedral 2:1 layer-type clay minerals. *Journal of Physical Chemistry B., 108*, 9685–9694.

Stevenson, C. M., & Gurnick, M. (2016). Structural collapse in kaolinite, montmorillonite and illite clay and its role in the ceramic rehydroxylation dating of low-fired earthenware. *Journal of Archaeological Science, 69*, 54–63.

Stucki, J. W. (1988). Structural iron in smectites. In: Stucki, J. W., Goodman, B. A., & Schwertmann, U. (Eds.), *Iron in Soils and Clay Minerals* (Chap. 17, pp. 625–664). NATO ASI Series, vol 217. Dordrecht: Springer. https://doi.org/10.1007/978-94-009-4007-9

Stucki, J.W., Bish, D., & Mumpton, F.A. (1990). *Thermal Analysis in Clay Science*. The Clay Minerals Society CMS Workshop Lectures (vol. 3)

Szymański, W., Drewnik, M., Stolarczyk, M., Musielok, Ł, Gus-Stolarczyk, M., & Skiba, M. (2022). Occurrence and stability of organic intercalation in clay minerals from permafrost-affected soils in the High Arctic – A case study from Spitsbergen (Svalbard). *Geoderma, 408*, 115591.

Vieillard, P., Gailhanou, H., Lassin, A., Blanc, P., Bloch, E., Gaboreau, S., Fialips, C. I., & Made, B. (2019). A predictive model of thermodynamic entities of hydration for smectites: Application to the formation properties of smectites. *Applied Geochemistry, 110*, 104423.

Vogels, R. J. M. J., Kloprogge, J. T., Geus, J. W., & Beers, A. W. F. (2005). Synthesis and characterization of saponite clays: Part 2. *Thermal Stability. American Mineralogist, 90*(5–6), 945–953.

Vyazovkin, S. (2015). *Isoconversional kinetics of thermally stimulated processes*. Springer.

Vyazovkin, S. (2021). Determining Preexponential Factor in Model-Free Kinetic Methods: How and Why? *Molecules, 26*(11), 3077.

Vyazovkin, S., Burnham, A. K., Criado, J. M., Pérez-Maqueda, L. A., Popescu, C., & Sbirrazzuoli, N. (2011). ICTAC

Kinetics Committee recommendations for performing kinetic computations on thermal analysis data. *Thermochimica acta, 520*(1–2), 1–19.

Vyazovkin, S., Burnham, A. K., Favergeon, L., Koga, N., Moukhina, E., Pérez-Maqueda, L. A., & Sbirrazzuoli, N. (2020). ICTAC Kinetics Committee recommendations for analysis of multi-step kinetics. *Thermochimica Acta, 689*, 178597.

Webb, S. W., Stanley, D. A., & Scheiner, B. J. (1986). Thermal analysis of ion-exchanged montmorillonite. *Particulate Science and Technology, 4*(2), 131–42.

Wicks, F. J. & Ramik, R. A. (1990). Vacuum Thermogravimetric Analysis and Evolved Gas Analysis by Mass Spectrometry. In Stucki, J. W., Bish, D., & Mumpton F. A. (Eds.), CMS Workshop Lectures, vol. 3. *Thermal Analysis in Clay Science*. The Clay Minerals Society. https://doi.org/10.1346/CMS-WLS-3.5

Wilson, M. A., Carter, M. A., Hall, C., Hoff, W. D., Ince, C., Savage, S. D., McKay, B., & Betts, I. M. (2009). Dating fired-clay ceramics using long-term power law rehydroxylation kinetics. *Proceedings of the Royal Society A: Mathematical, Physical and Engineering Sciences, 465*(2108), 2407–2415.

Wolters, F., & Emmerich, K. (2007). Thermal reactions of smectites—Relation of dehydroxylation temperature to octahedral structure. *Thermochimica Acta, 462*(1–2), 80–88.

Xi, Y., Martens, W., He, H., & Frost, R. L. (2005). Thermogravimetric analysis of organoclays intercalated with the surfactant octadecyltrimethylammonium bromide. *Journal of Thermal Analysis and Calorimetry, 81*(1), 91–97.

Yariv, S., Borisover, M., & Lapides, I. (2011). Few introducing comments on the thermal analysis of organoclays. *Journal of Thermal Analysis and Calorimetry, 105*(3), 897–906.

Zabat, M., & Van Damme, H. (2000). Evaluation of the energy barrier for dehydration of homoionic (Li, Na, Cs, Mg, Ca, Ba, $Al_x(OH)_y^{z+}$ and La)-montmorillonite by a differentiation method. *Clay Minerals, 35*(2), 357–363.